International Journal of Applied Earth Observations and Geoinformation 102 (2021) 102419

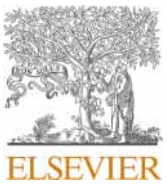

Contents lists available at ScienceDirect

International Journal of Applied Earth Observations and Geoinformation

journal homepage: www.elsevier.com/locate/jag

# Mapping coastal marine ecosystems of the National Park of Banc d'Arguin (PNBA) in Mauritania using Sentinel-2 imagery

A. Pottier [a,b,*], T. Catry [b], E. Trégarot [c], J.-P. Maréchal [d], V. Fayad [e], G. David [b], M. Sidi Cheikh [f], P. Failler [c]

[a] SENS, IRD, CIRAD, Univ Paul Valery Montpellier 3, Univ Montpellier, Montpellier, France
[b] ESPACE-DEV, Univ Montpellier, IRD, Univ Antilles, Univ Guyane, Univ Réunion, Montpellier, France
[c] Centre for Blue Governance, Department of Economics and Finance, Portsmouth Business School, University of Portsmouth, Richmond Building, Portland Street, Portsmouth PO1 3DE, United Kingdom
[d] Nova Blue Environment, 14 rue Chéry Rosette, 97233 Schoelcher, Martinique, France
[e] Humming Drone, 135 rue Lamartine, 97200 Fort de France, Martinique, France
[f] Conservation Ecology Group, Groningen Institute for Evolutionary Life Sciences, University of Groningen, P.O. Box 11103, 9700 CC Groningen, the Netherlands

ARTICLE INFO

*Keywords:*
Coastal marine ecosystems
Seagrass
Remote sensing
Sentinel-2
SPOT-6
Banc d'Arguin

ABSTRACT

Coastal marine ecosystems ensure fundamental hydro-ecological functions and support high levels of biodiversity, besides being an important resource for local populations. These biocenosis have been increasingly threatened by human pressures (e.g. pollution, overfishing) along with climate change, which may have a dramatic impact on them. The National Park of Banc d'Arguin (PNBA) in Mauritania, one of the biggest parks in Western Africa, is a RAMSAR zone (classified by UNESCO since 1989) that plays a major role in (i) the maintenance of marine biocenosis, (ii) the protection of the ecosystems and (iii) the sequestration of carbon dioxide. Ecosystem databases and associated maps of the PNBA are out of date and limited to the southern and central parts of the park: updating is thus needed. In this paper, a supervised Support Vector Machine (SVM) was deployed using high-resolution images from Sentinel-2 combined with field data to map marine biocenosis of the PNBA. The results highlight that Sentinel-2 shows good classification accuracy for mapping marine biocenosis (>80% overall accuracy and a kappa index of 0.75), including seagrass beds. Also, the use of high-resolution sensors like SPOT-6 (1.5 m pixels) can overcome the limitations of Sentinel-2 (10 m pixels) when it comes to detecting small ecosystems distributed in patches. The use of freely-downloadable Sentinel-2 data, processed using geoinformatic freeware, make the methodology reproducible, affordable and easily transferable to local actors of biodiversity conservation for long term usage.

## 1. Introduction

Seagrass habitats offer a wide variety of services essential for local populations, in particular for subsistence fishing (Nagelkerken et al. 2002), in West Africa (de la Torre-Castro and Rönnbäck, 2004). They also ensure fundamental hydro-ecological functions such as sediment stabilization and protection of the coastline from erosion by reducing the strength of waves and tidal current energy (Barbier et al., 2011; Chen et al., 2007; Ondiviela et al., 2014), cycling of nutrients (Duarte, 1990; Evrard et al., 2005; Romero et al., 2006) and carbon (Duarte et al., 2010; Fourqurean et al., 2012; Kennedy et al., 2010), and support of high-level biodiversity (Coll et al., 2010; Unsworth and Cullen-Unsworth, 2014). Despite their importance, seagrass beds are particularly threatened, resulting in a degradation of their habitat and a decline in their global surface for the past decades (Duarte, 2002; Orth et al., 2006; Waycott et al., 2009). The degradation of seagrass meadows is a complex process caused by several interlinked variables, coming both from anthropic (pollution, resource overexploitation, landscape change, etc.) and environmental pressures (geological events, biological interactions such as sediment bioturbation or disease (Short and Wyllie-Echeverria, 1996); sea-level change, physical modification of coastlines, and global changes in atmospheric CO2 concentration and water temperature (Orth et al. 2006); extreme climate events (McKenzie and Yoshida, 2020); marine heat waves (Strydom et al., 2020)), making it a difficult

* Corresponding author at: UMR SENS, Rue du Professeur Henri Serre, 34090 Montpellier, France.
*E-mail address:* aurea.pottier@ird.fr (A. Pottier).

https://doi.org/10.1016/j.jag.2021.102419
Received 31 March 2021; Received in revised form 11 June 2021; Accepted 25 June 2021
Available online 16 July 2021

process to monitor and understand. Given the importance of this complex ecosystem, the conservation status of seagrass beds is considered an effective indicator for the overall health of marine and coastal ecosystems.

Remote sensing has been used for decades to monitor the spatio-temporal evolution of these ecosystems (Hossain and Hashim, 2019; Hossain et al., 2015; Short and Coles, 2001). Seagrass beds have been monitored using various remote sensing data such as aerial photography (Ferguson et al., 1993; Kendrick et al., 2002; Kirkman, 1996), satellite imagery (Kovacs et al., 2018; Lyons et al., 2011, 2013; Pu and Bell, 2017; Topouzelis et al., 2018; Yang et al., 2017) and, more recently, drone imagery (Phinn et al., 2018). Authors highlight difficulties they have encountered to map seagrass beds due to the complexity and diversity of the local environment which represent a big challenge, in particular, the difficulty to separate seagrass from other classes and among each other. Indeed, the presence of the water column and its own characteristics (depth, color, turbidity, sediment content, etc.) have a significant impact on the absorption of the spectral signatures of the seagrass and cause confusions (Dobson, 1995; Green et al., 1996; Kovacs et al., 2018; Kutser et al., 2003, 2020; Lee and Carder, 2002; McKenzie et al., 2001; Phinn et al., 2008; Vahtmäe et al., 2020). Only a few of these studies relate to West Africa, where there is still limited knowledge of seagrass distribution and their evolution, though this information is an essential prerequisite for assessing the ecosystem services seagrass beds provide. Furthermore, these data are often outdated and fragmented, which is the case for the National Park of Banc d'Arguin (PNBA) in Mauritania.

Maps of the distribution of marine biocenosis of the PNBA have already been produced within the framework of the PACOBA project (Projet d'Approfondissement des connaissances scientifiques de l'écosystème du Golfe du Banc d'Arguin, 2012) from SPOT-5 images of 2003 and 2007. However, cartographic knowledge and ecosystems distribution are outdated, limited to the southern and central parts of the park, and details on the methods and the accuracy of their results are insufficient. It is therefore necessary to update the ecosystem mapping of the PNBA with an approach that can be easily implemented for long-term monitoring. In this study, we propose an approach using Sentinel-2 images combined with field data (more than 500 points) to map marine biocenosis of the PNBA, with a particular interest for seagrasses. We aim at developing a methodology for processing these data, easily replicable by local conservation agencies for future map updates and assessment of ecosystem services.

## 2. Study area and data

### 2.1. Study area

The PNBA is a natural reserve in Mauritania, founded in 1976 by the President of the Islamic Republic of Mauritania, Mokhtar Ould Daddah, in consultation with the French naturalist Theodore Monod (Ould Cheikh 2002a,b). Covering a third of the Mauritania coastline, it extends from Pointe Minou in the north (beyond Cape Arguin) to the village of Mamghar in the south (beyond Cape Timiris), and includes the islands of Arguin and Tidra. The PNBA covers 12 000 km$^2$, divided between the maritime part (the Atlantic Ocean) and the continental part (the Sahara Desert, Fig. 1) and is, therefore, one of the largest natural reserve in West Africa. The PNBA is characterized by high productivity, sustained by the enriched coastal waters, due to the upwelling offshore and wind-driven Sahara dust (Demarcq and Faure 2000). For the high productivity, the diversity of coastal marine habitats, and their importance for a large population of migrating birds, the PNBA was recognized as a RAMSAR site in 1982 and a UNESCO World Heritage Site in 1989. Tidal marshes

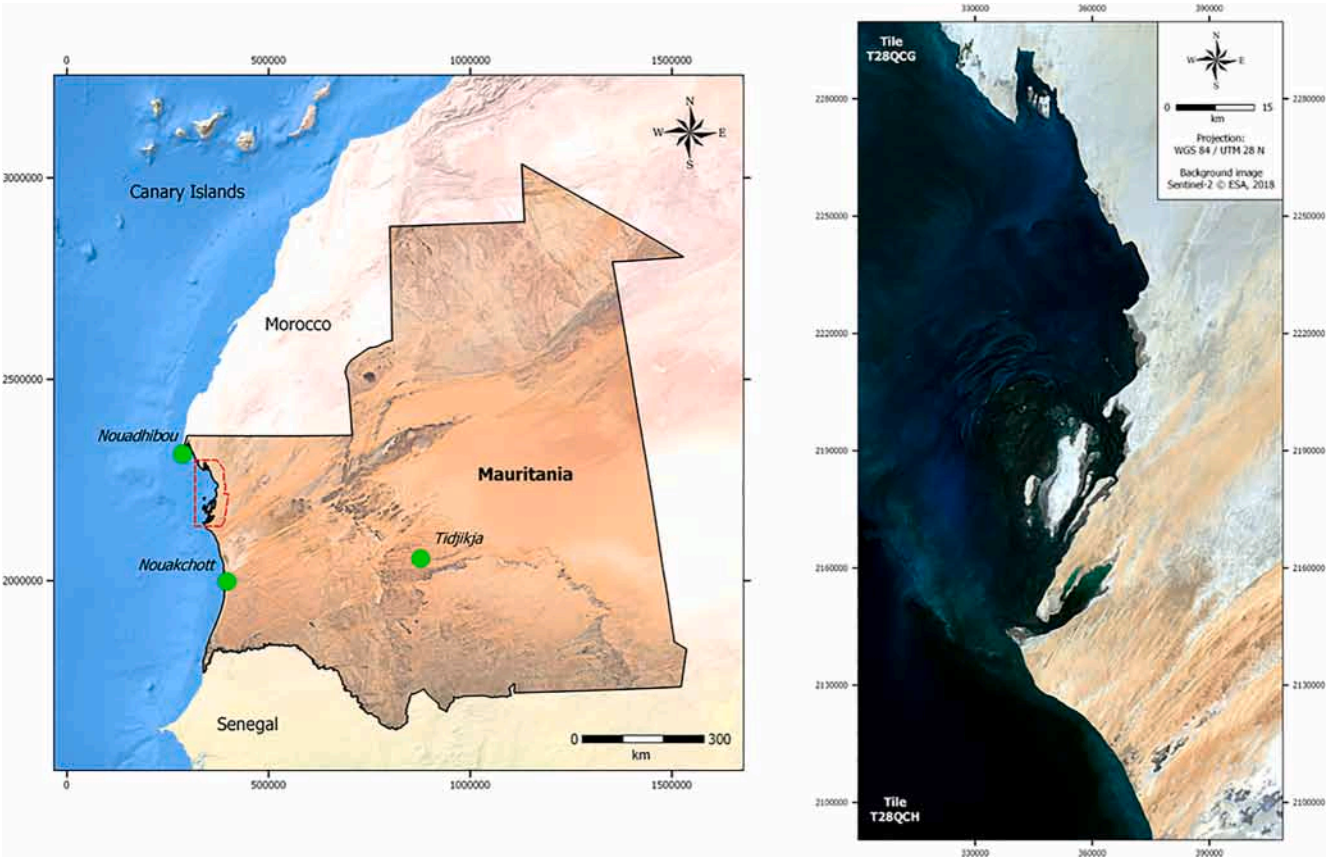


**Fig. 1.** Study area, showing the extent of the PNBA in Mauritania (on the left, background made with Natural Earth. Free vector and raster map data @ naturalearthdata.com) and the mosaic of the Sentinel-2 images (on the right).

in the PNBA constitute a unique ecosystem with the very northernmost mangrove formations (*Avicennia germinans*) and southernmost spartina meadows (*Spartina maritima*) in West Africa (Lebigre, 1991). The northern part of the PNBA shelters habitats for the meagre (*Argyrosomus regius*) and *elasmobranchii* species (sharks and rays), which are particularly abundant in the waters of the park (Revillion, 2010; Revillion et al., 2011; Sevrin Reyssac and Richer de Forges, 1985), though difficult to map by satellite images because of the depth and turbidity of these areas. Intertidal areas cover much of the southern part of the PNBA; they are composed of shallow mudflats, crossed by channels and largely covered with seagrass beds (*Eelgrass*: *Zostera noltii* and *Cymodocea*: *Cymodocea nodosa*).

The Park plays a crucial role in the protection of those ecosystems and the provision of associated services in the Gulf d'Arguin. Indeed, the Park is essential for the renewal of fisheries resources in the exclusive economic zone of Mauritania (Guénette et al., 2014) and more broadly at a sub-regional level and in the sequestration of atmospheric carbon in a country with low terrestrial vegetation. Conservation of the natural environment and sustainable development of populations are the main objectives of the PNBA.

### 2.2. Satellite images

Satellite images were acquired at low tide, as much as possible during a high coefficient tide, for two reasons:

- a large part of the intertidal seagrass meadows emerged;
- for subtidal seagrass beds, the water depth was smaller, which minimizes the effect of absorption of the spectral wavelength by water and thus facilitated their detection.

Given the size of the PNBA, two Sentinel-2 images (tiles T28QCG and T28QCH, 10 m spatial resolution, Fig. 2) of the 22 February 2018, taken at low tide (0.5 m at 11 h33, time of acquisition), were used to cover the entire park and to identify marine and terrestrial ecosystems, including intertidal seagrass beds, mudflats, salt marshes, and mangroves. Although less spatially resolved than the SPOT-5 image from 2007 (2.5 m) used in the PACOBA project, with a resolution of 10–60 m depending on the spectral bands (Table 1), Sentinel-2 images have the advantage of being easily accessible and at no cost with a 12-day revisit time over Mauritania providing access to optimal cloud and tidal conditions, for regular updating of the maps produced in the framework of this project, and requiring limited computing resources for the processing of the data. In addition, we also downloaded 4 more Sentinel-2 images on our study area between December 2017 and February 2018 (12/09/2017, 12/24/2017, 01/08/2018, 02/27/2018) to test the robustness of the method on the maritime part, focusing on seagrass. Images were chosen according to match different criteria: tide coefficient (around 0.5 m tidal height, in order to maximum water transparency, minimum sun and sky glint), cloud cover (<0.5%) and period of acquisition (close to the field mission with a small gap between dates). The choice to use images with a short-range period between acquisitions is to ensure the stability of meadows at this period since this kind of ecosystem can have an important spatio-temporal variation in a short laps of time, especially in case of high tides or storm.

### 2.3. Turbidity and bathymetric products

A bathymetric map was provided by the Mauritanian Institute of Oceanographic Research and Fisheries (*French*: Institut Mauritanien de Recherches Océanographiques et de Pêches, IMROP). This product consisted of a bathymetric survey every 5 m and was intended to be used to correct water column on the image, based on a modeling approach linking the measured luminance to the parameters of the target (meadows or/and substrate), to the parameters of the water interposed between the sensor and the target. This physical approach would have required:

- a model of the bottom depth (related to bathymetry and tides)
- an attenuation model of irradiance and reflected signal depending on the water column and turbidity

However, the resolution of the bathymetric product was not sufficient to be effectively exploited for mapping purposes using satellite images with a resolution of 10 m since the intertidal zone ranges from 0 to 5 m and it would have required measurements of seagrass spectral signature in water. Therefore, the bathymetric product was only used to exclude areas deeper than 10 m, where seagrass beds are less likely to be present given the local turbidity.

In theory, turbidity effects should also have been corrected during the pre-processing of Sentinel-2 data using turbidity products. However, water turbidity depends on the strong spatio-temporal variation related to the seasonal cycle of phytoplankton growth (phytoplankton blooms), the upwelling phenomenon, and the presence of strong currents generated by the filling and emptying of the bay during the tidal cycle. Thus, it is very difficult to correct for water turbidity due to the multiplicity of phenomena involved. That is why we chose the 5 Sentinel 2 images to work with very carefully in order to minimize such effects, by favoring low tide images (with high tide coefficient) with maximum water transparency. This is made possible by the temporal repeatability of Sentinel-2 acquisitions. Yet, when some corrections are needed, there are now various method available to map water quality (Chl-a, CDOM, TSS, turbidity…) with Sentinel 2 (Al-Kharusi et al., 2020; Bramich et al., 2021; Caballero and Stumpf, 2020; Sòria-Perpinyà et al., 2021; Vahtmäe et al., 2020).

**Table 1**
The spectral band features of the Sentinel-2 sensor.

| | | S2A | | S2B | | |
|---|---|---|---|---|---|---|
| **Band Number** | **Band Name** | **Central wavelength (nm)** | **Bandwidth (nm)** | **Central wavelength (nm)** | **Bandwidth (nm)** | **Spatial resolution (m)** |
| **1** | *Coastal aerosol* | 442.7 | 21 | 442.3 | 21 | 60 |
| **2** | *Blue* | 492.4 | 66 | 492.1 | 66 | 10 |
| **3** | *Green* | 559.8 | 36 | 559.0 | 36 | 10 |
| **4** | *Red* | 664.6 | 31 | 665.0 | 31 | 10 |
| **5** | *Vegetation red edge* | 704.1 | 15 | 703.8 | 16 | 20 |
| **6** | *Vegetation red edge* | 740.5 | 15 | 739.1 | 15 | 20 |
| **7** | *Vegetation red edge* | 782.8 | 20 | 779.7 | 20 | 20 |
| **8** | *NIR* | 832.8 | 106 | 833.0 | 106 | 10 |
| **8A** | *Narrow NIR* | 864.7 | 21 | 864.0 | 22 | 20 |
| **9** | *Water vapour* | 945.1 | 20 | 943.2 | 21 | 60 |
| **10** | *SWIR - Cirrus* | 1373.5 | 31 | 1376.9 | 30 | 60 |
| **11** | *SWIR* | 1613.7 | 91 | 1610.4 | 94 | 20 |
| **12** | *SWIR* | 2202.4 | 175 | 2185.7 | 185 | 20 |

### 2.4. Field data

Marine and terrestrial ecosystems were sampled during a field mission carried out from 8 to 25 April 2018 (Fig. 2). We collected approximately 500 points on the field (Table 2), 311 of which on the marine part (classes 1, 2, 5 and 6 on the land cover classification) and 214 on the intertidal area (classes 3, 4 and 7 on the land cover classification). 70% of these points were used as a training sample and 30% were used to validate cartographic observations from satellite images. To select the training sample, we used the random selection tool of QGIS, which allows to select random points in a layer for each class based on a certain percentage. An overview of the basic statistics of these field datasets was computed, as boxplots, using R language on R Studio and can be seen in the result section. To compute these statistics, all the points (both training and validation points) were used. We also collected about 30 points on the terrestrial area (classes 8, 9 and 10) that were also used to train the algorithm but not for the accuracy since it was not the main purpose of the study. Though the terrestrial part of the PNBA was not a major issue for our study, we decided to use the points acquired in the field in order to enhance the value of datasets.

The sampling strategy was driven by the size of the PNBA and the availability of cars and boats to cover the larger area possible. Since we had a limited access to such vehicles, the sampling can seem limited in coverage and heterogeneous since some points are gathered in limited geographical areas (Fig. 2a). The heterogeneity in the number of samples per class is also the reflection of class distribution on the ground. For instance, the geographical extent of mangroves is extremely limited compared to the extent of seagrass. However, a particular interest was dedicated to the northern part of the park that was poorly known.

On the field, for each point we sampled, the location was registered using a Garmin GPSMAP 65 series and the type of land cover reported. For seagrass, a qualitative assessment of the density was also carried out, using a 3 class qualitative description: low-density, medium density and high density.

## 3. Method

To map the entire extent of the PNBA, we used the image of the 22 February 2018. Then, for the four other dates, only the maritime part was mapped in order to assess the robustness of the method for mapping seagrass. The classification process applied on Sentinel-2 imagery for the mapping of marine and terrestrial ecosystems of the PNBA is presented in Fig. 3. Pre-processing and processing steps of the Sentinel-2 imagery used in this study were carried out on free software such as R (R Core Team, 2019), Orfeo Toolbox and QGIS.

Level 1C Sentinel-2 data were downloaded on the Copernicus Open Access Hub (https://scihub.copernicus.eu/dhus/#/home). Atmospheric corrections and production of level 2A data were performed using the processor ACOLITE (Atmospheric correction for OLI 'lite') developed by the Royal Belgian Institute of Natural Sciences (Vanhellemont and Ruddick, 2018; Vanhellemont, 2019). ACOLITE combines the atmospheric correction algorithms for aquatic applications of Landsat and Sentinel-2 as well as other sensors, and was released to the public in April 2021. ACOLITE allows simple and fast processing of imagery from various satellites, including Sentinel-2/MSI (A/B), for coastal and inland water applications. The Dark Spectrum Fitting atmospheric correction algorithm works especially well for turbid and productive waters, but can also be applied over clear waters (https://github.com/acolite/acolite). Pereira-Sandoval et al. (2019) evaluated different methods for the preprocessing of Sentinel-2 data for applications regarding shallow waters. Comparing in situ measurements and satellite reflectance, they showed that processors like ACOLITE perform well in complex environments like hypertrophic or meso-trophic environments. This the case of the PNBA, an area where a strong oceanic dynamic occurs with the Mauritanian upwelling and sedimentary contribution from the Sahara affecting coastal waters. Besides, ACOLITE also enables the resampling of the data at 10 m resolution and the merging of the 2 tiles into one single image.

Spectral signatures for each class were extracted from the 4 spectral bands (NIR, red, green and blue) of the Sentinel-2 image of the 22 February 2018 using the field points on R Studio and summarize as boxplots (Frigge et al., 1989; Williamson et al., 1989).

To map the marine ecosystems of the PNBA, we only used 4 bands of the Sentinel-2 sensor: Near Infrared (NIR), red, green and blue bands. Indeed, visible bands (red, green, and blue) are the only bands that are not completely absorbed by water, contrary to NIR or short-wave infrared (SWIR) that are absorbed even in shallow water (Dekker et al., 2007; Hossain et al., 2015). NIR band was only used to compute the normalized difference water index - NDWI (McFeeters, 1996) and the normalized difference vegetation index - NDVI (Rouse et al., 1974; Tucker et al., 1979). Both Sentinel-2 tiles were pre-processed similarly and, in order to minimize computing resources and processing times, calculations were limited to the geographical extent of the PNBA (Fig. 2). The 10 m bathymetric contour line was also used offshore to delimitate the extent of the area where seagrass is likely to be present (below 10 m in depth, turbidity is too high to allow seagrass growth in the Banc d'Arguin).

NDVI and NDWI were used to create three masks over the park: a 'water' mask containing the marine part including the subtidal and intertidal flats, a 'land' mask containing the continental part of the park and a 'transition' mask corresponding to the buffer area between marine and terrestrial areas of the park (including mangrove, sebkha and salt marsh ecosystems). These masks help to reduce radiometric confusion in this complex environment, thus increasing the accuracy between classes. Besides, the role of these masks was also to minimize computing resources and processing times by not processing all the extent of the park at a time but zone by zone. Finally, it also allowed us to focus on the areas we were interested in: maritime part where seagrasses are located and, to a lesser extent, the intertidal part where you can find the mangroves.

We performed supervised classifications on each of those three masks using the SVM (Support Vector Machine) algorithm on the open-source software Orfeo Toolbox. SVM is a widely used machine learning algorithm in remote sensing. The SVM algorithm was first developed for statistical purpose (Vapnik, 1995) and its use in remote sensing began to grow in the 2000s and increased in the late 2000s (Mountrakis et al. 2011). SVM algorithm aims to find the optimal hyperplane of the training samples to separate classes between them. Thus, the algorithm will try to maximize the margin between the samples and the hyperplane separator to minimize classification errors. We made the choice to use SVM rather than another supervised machine learning algorithm for 4 reasons: (1) the functioning of SVM allows to use few training points while guaranteeing good results (Foody and Mathur, 2004a); (2) SVM method often gives good results in complex and noisy data (Poursanidis et al., 2018); (3) several recent studies on mapping optically shallow habitats were carried out using SVM and showed good results accuracy so we also used SVM classifier (Bakirman et al., 2016; Eugenio et al., 2015; Poursanidis et al., 2018, 2019; Traganos and Reinartz, 2018; Traganos et al., 2017, 2018; Zhang, 2015); and (4) some of these studies showed that SVM performed better results than RF or Maximum Likelihood (Traganos and Reinartz, 2018; Traganos et al., 2018) while other studies (not on seagrass, though) also showed that SVM can be more accurate than popular contemporary techniques such as neural networks and decision trees as well as conventional probabilistic classifiers such as the maximum likelihood classification (Foody and Mathur, 2004b; Huang et al., 2002). For our classifications, 70% of the field samples were used as training data and 30% for validation. For the "water" part, we only used the red, green, and blue bands to limit spectral wave absorption by water, while the SVM classifier was performed on the three bands plus the near-infrared band for the "transition" and "land" part. Then, we merged the three classifications to produce a 10-classes map of the ecosystems of the PNBA, including the two species of seagrass,

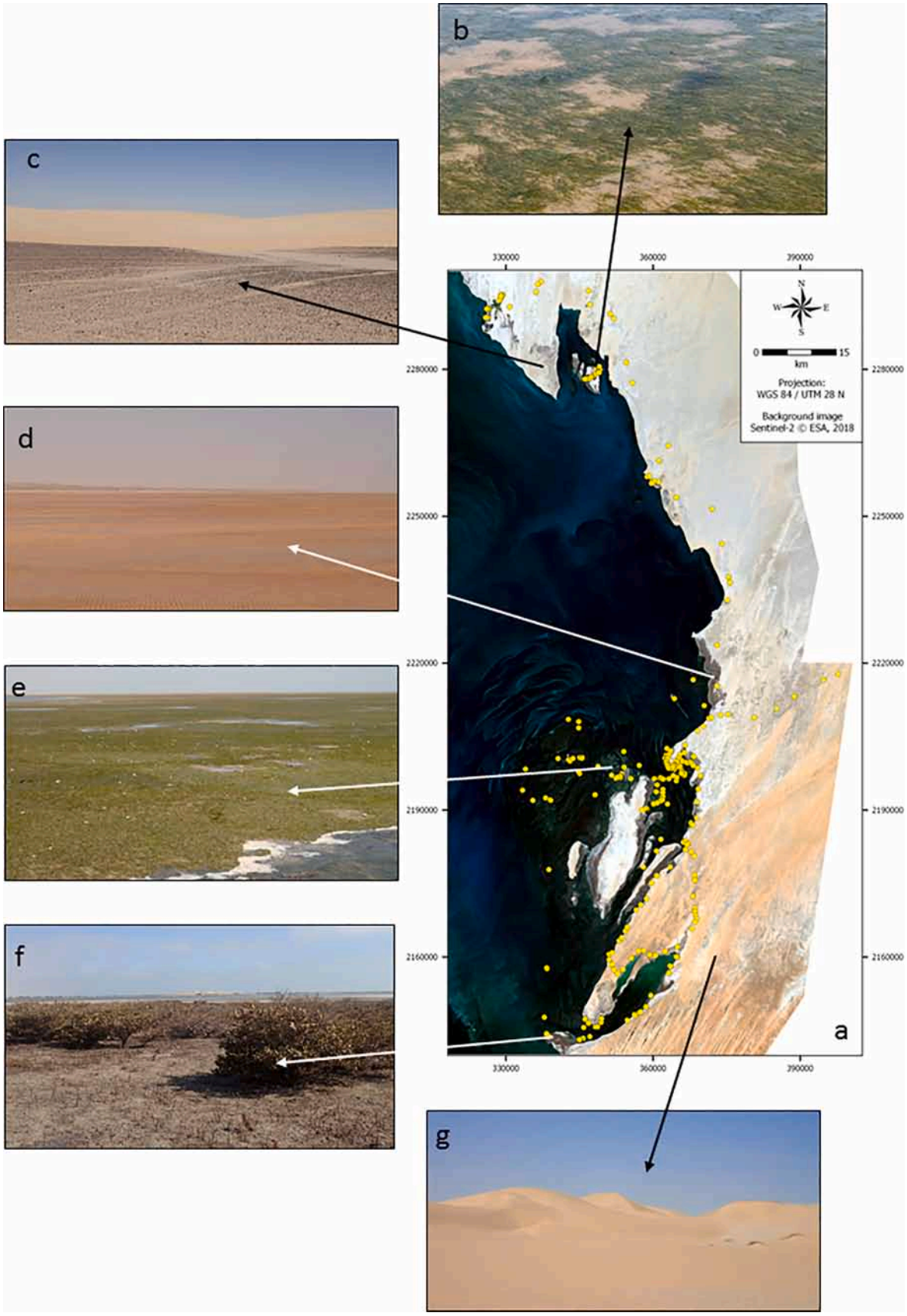


**Fig. 2.** a- Field sampling (yellow dots) on marine and terrestrial ecosystems in the National Park of Banc d'Arguin (PNBA), including a total of more than 500 points; b- seagrass beds (*Cymodocea nodosa*); c- rocky sand, d- sebkha (flat-bottomed depressions, generally floodable, where salty soils limit the development of vegetation); e- seagrass beds (*Zostera noltii*); f- mangrove; g- dune cord. (For interpretation of the references to color in this figure legend, the reader is referred to the web version of this article.)

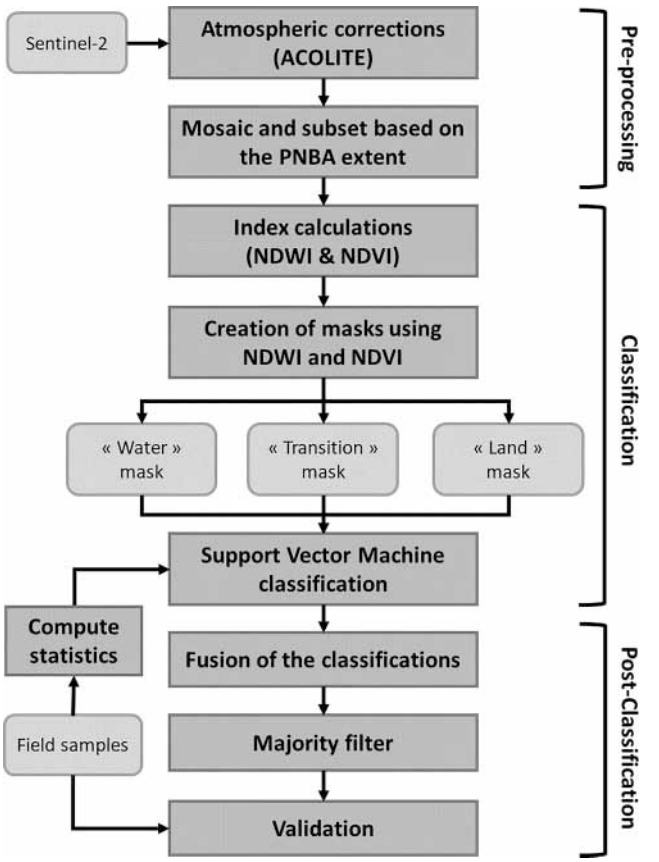


**Fig. 3.** Classification process applied on Sentinel-2 imagery for the mapping of the ecosystems of the National Park of Banc d'Arguin, Mauritania.

**Table 2**
Details of samples acquired during field mission.

| Class | Total number of points | Number of points used for training | Number of points used for validation |
|---|---|---|---|
| **Seagrass *Cymodocea* (1)** | 115 | 75 | 40 |
| **Seagrass *Zostera* (2)** | 102 | 65 | 37 |
| **Mangroves (3)** | 62 | 40 | 22 |
| **Salt marshes (4)** | 75 | 50 | 25 |
| **Mudflats (5)** | 50 | 35 | 15 |
| **Intertidal bare sediments (6)** | 43 | 30 | 13 |
| **Sebkha (7)** | 69 | 45 | 24 |
| **Bare sand (8)** | 15 | 15 | – |
| **Sandy soil with vegetation more or less dense (9)** | 7 | 7 | – |
| **Rocky Sand (10)** | 8 | 8 | – |

mangroves, salt marshes, mudflats, bare intertidal sediments, sebkha, bare sand, vegetated sand and rocky sand (Fig. 5). Finally, we applied a majority filter on the classification to eliminate over-detection due to isolated pixels.

In addition, we also performed supervised classification using the SVM classifier, only on the maritime part, for the images of the 9 December 2017, the 24 December 2017, the 8 January 2018 and the 27 February 2018. This additional step was in order to assess the robustness of the method for mapping seagrass. We decided not to restart classifications on all the extent of the PNBA for 3 reasons: (1) the study focuses mainly on seagrass; (2) other classes like mangroves, salt marshes or sebkha do not change a lot in such a short time; (3) time saving.

The last important step before validating the classifications was to assess its accuracy using a confusion matrix (Congalton and Green, 1999; Congalton, 1991). This process will compute an error matrix giving the information about accuracy, F-score and Recall of each class as well as the overall accuracy and the Kappa index (Landis and Koch, 1977; Cohen, 1960) of the classification. As discussed in section 2.4, we used 30% of the samples to compute the confusion matrix. The confusion matrix was calculated for all the classes (exept those of the terrestrial part) for the image of the 22 February 2018 and only on the maritime part for the other classifications.

## 4. Results

### 4.1. Field sample statistics

The spectral signatures of the 7 classes of the classification were extracted from the 4 spectral bands (NIR, red, green and blue) of Sentinel-2 image (22 February 2018) to show the spectral separability among them and are visible in Fig. 4 below (Fig. 4).

These statistics showed that seagrass *Zostera* and seagrass *Cymodocea* have very close spectral responses in the 4 spectral bands except in the NIR band. In the visible bands, we observed close responses with some variability in the red part of the spectrum, as it has also been shown in other studies (Kutser et al., 2006, 2020; Matta et al., 2014; Roelfsema, unpublished; Vahtmäe et al., 2006). They also showed that both species have very close spectral responses in the green and blue band but less in the red band. Thus, it is practically impossible to separate these species using only multispectral data (2020;; Paringit et al., 2003).

For the other classes, we observed close spectral responses between mangroves and salt marshes except in the red band. However, the two ecosystems occur together at the same locations with a low spatial distribution, where mangroves are often in small patches of small density. Thus, it can be difficult to separate the two ecosystem at this resolution due to mixed pixel. For mudflat, we observed some similar spectral responses with intertidal bare sediment in the NIR and red band but less in the green and blue band. Both ecosystem should be differentiable, though they might be some confusion. Finally, Sebka showed important spectral responses with all the classes except for some similarities with interdial bare sediment. However, since we used masks to separate the maritime part and the intertidal part, there should not be confusion between these two classes.

### 4.2. Classification

We produced a 10-class land cover map of the marine and terrestrial ecosystems of the PNBA (Mauritania) for the image of the 22 February 2018. While previous studies of the marine ecosystems of the park only focused on the central area, around Tidra island (see results from PACOBA), we mapped the entire extent of the park (Fig. 5) updating knowledge on the distribution of seagrass species and other ecosystems to the northern (Agadir, Fig. 6a) and southern (Mamghar, Fig. 7a) areas. We also produced 4 land cover maps of 4 classes (seagrass *Cymodocea*, seagrass *Zostera*, mudflat and intertidal bare sediment) on the maritime part, one for each other date (12/09/2017, 12/24/2017, 01/08/2018 and 02/27/2018).

Most of the seagrass beds are distributed around the central island of Tidra. *Zostera noltii* beds were identified on flats at low tide (Fig. 6b), *Cymodocea* were located in areas covered in water like the edges of the channels (Fig. 7c) and small intertidal ponds (Fig. 6c) on the flat areas at low tide. Both species are submerged at high tide, making them difficult to detect, if not impossible. The distribution of mangrove forests is extremely limited with small patches north of Mamghar and Tidra (Fig. 7a, 7b and 7d). Finally, the transition areas between sandy land and seagrass, as found around Tidra Island or in the southern part of the park, are composed of mudflats, salt marshes (Fig. 7e) and sebkhas, which are flood topographic flat-bottomed depressions in which the

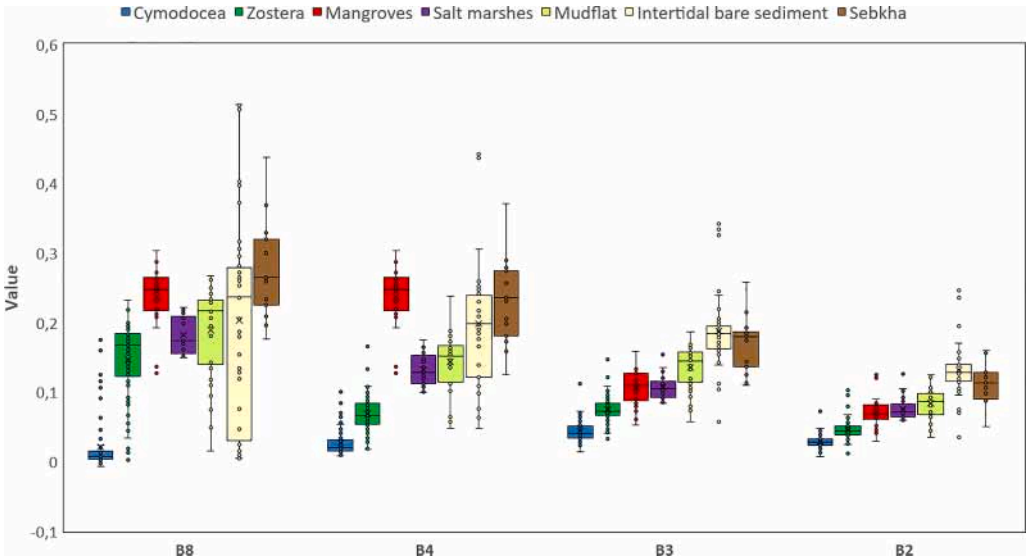


**Fig. 4.** Boxplots showing the statistics of the 7 classes on the 4 spectral bands for the image of the 22 February 2018. B8: Near Infrared; B4: red; B3: green; B2: blue. (For interpretation of the references to color in this figure legend, the reader is referred to the web version of this article.)

growth of vegetation is limited by salty soils.

Using the confusion matrix, for the classification of the 22 February 2018 in 7 classes, we assessed the overall accuracy of the classification to 71.6% with a Kappa index of 0.66 (Table 3). For the same date but without distinctition of seagrass (Class 1 and 2 were merged), we obtained an overall accuracy of 86.8% and a Kappa index of 0.82 for the classification (Table 3). Both results are satisfying given the environment's complexity of the study area.

For the 5 classifcations on the maritime part with seagrass *Cymodocea* and *Zostera* separated, we assessed the average of the overall accuracy of 63.8% with a minimum of 62.5% and a maximum of 69.2% and an average kappa index of 0.47 with a minimum of 0.45 and a maximum of 0.55 (Table 4). For the 5 classifications, we assessed the average of the overall accuracy of 92.7 with a minimum of 91.3% and a maximum of 95.2% and an average kappa index of 0.82 with a minimum of 0.78 and a maximum of 0.88 (Table 5). Other detailed confusion matrices can be found in the supplementary material.

A comparison between a SPOT-5 image from 2003 used in the PACOBA project and the Sentinel-2 image of February 2018 evidences the variability in the spatial distribution of the seagrass, especially in the Tidra area (Fig. 8). The first image (Top) shows the SPOT-5 image from 2003 in false color where the seagrass appear in red while the second image (Bottom) shows the Sentinel-2 image from 2018 also in false color.

On the basis of the maps, we estimated the surfaces covered by each ecosystem. Reference values for the PNBA from previous studies were: 450 $km^2$ of *Zostera noltii*, 374 $km^2$ of *Cymodocea nodosa* and 5 $km^2$ of mangroves. The extents calculated in this study are presented in Table 6.

## 5. Discussion

### 5.1. Classification accuracy

Several confusion matrices were produced for the Sentinel-2 classifications, using Orfeo Toolbox, focusing on *Zostera noltii* and *Cymodocea nodosa* seagrass species, which were the primary targets of this research project. However, as we encountered some confusion between seagrass, salt marshes, and mangroves, we also considered those ecosystems for estimating the classification accuracy. Since the terrestrial area was not the main focus of our study, we did not take into account the 3 land classes in the accuracy assessment of the classification.

For the classification of the 22 February 2018, Sentinel-2 offered an overall accuracy of 95% with a recall of 1 and an F-score of 0.97 in the detection of seagrass (Table 3). Given the resolution of the images (10 m), the complexity of the seagrass ecosystem, and the variable size of patches observed on the field, we consider this result to be satisfactory. However, the intra-class classification of seagrass (i.e. the ability to discriminate the seagrass species) was less satisfying. Many confusions are identified between seagrass species and with other classes, in particular intertidal bare sediments. Indeed, *Zostera* reached 58.5% accuracy with a recall of 0.64 and an F-score of 0.61, while *Cymodocea* had an overall accuracy of 66.7% with a recall and F-score of 0.65 and 0.66 respectively. Several factors can explain this result: at a resolution of 10 m, in low-density seagrass beds, the substrate can contaminate the entire pixel, which is then attributed to the « intertidal bare sediment » class when it is, in reality, a mixed pixel. Radiometrically, the discrimination between the two species of seagrass is challenging at this resolution, accounting for the good overall accuracy of the seagrass class but the low intra-class accuracy. Moreover, although the images were acquired at low tide, part of the study area is still submerged. The presence of water induces radiometric disturbances causing misclassifications. It shows how important it is to take into account the presence of water on the image and to correct for the water disturbances on the signal, using bathymetry, turbidity, and tide models combined to in situ spectral measurements. None of these data were available in this study and we were not able to perform any of these corrections. This aspect would be a great improvement for future updates of the distribution of seagrass species in the PNBA.

We obtained 100% accuracy for mangroves, but the recall and F-score are only 0.32 and 0.48, respectively. These results mean that pixels proposed as mangroves by the classification are indeed mangroves, hence the 100% accuracy, but also that the classification missed a lot of mangrove pixels, resulting in a low recall and F-score. These results can be explained by the substantial confusion between mangroves and salt marshes since the two ecosystems occur together at the same locations, with limited distribution on relatively small surface areas, where mangroves are often in small patches of small density. The confusion matrix supports this theory since out of 22 mangrove points, 7 were correctly identified as mangroves, but 12 as salt marshes and the other points as mudflats and bare intertidal sediments. The reflectance of low-density mangroves was contaminated by the radiometric background of salt marshes, hence misclassifications. This explains why we only detected 0.5 $km^2$ of mangroves against the reference area of 5 $km^2$.

However, for salt marsh, we have a reliable recall of 0.8 but a

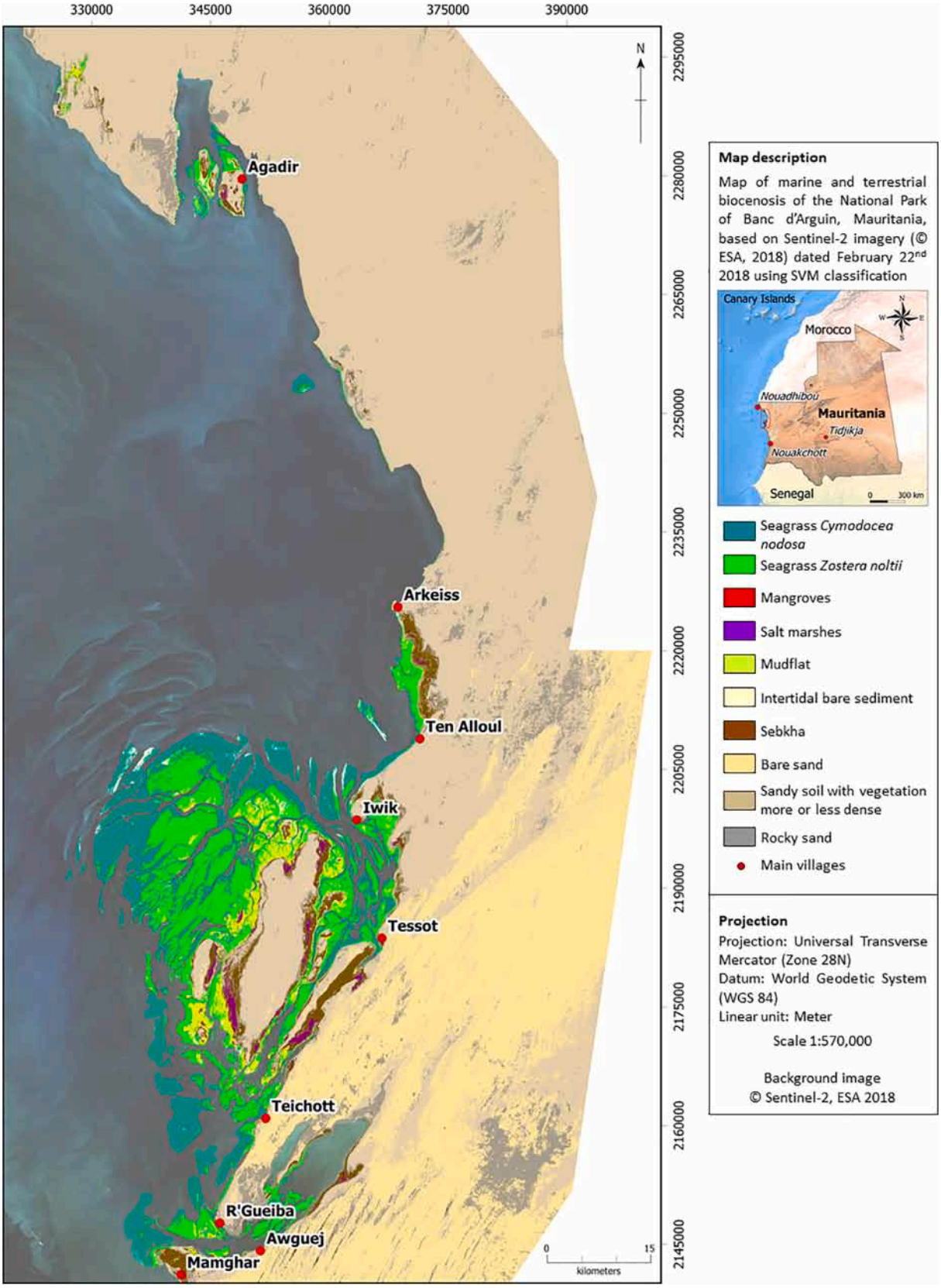


**Fig. 5.** Mapping of the entire extent of the National Park of Banc d'Arguin, Mauritania.

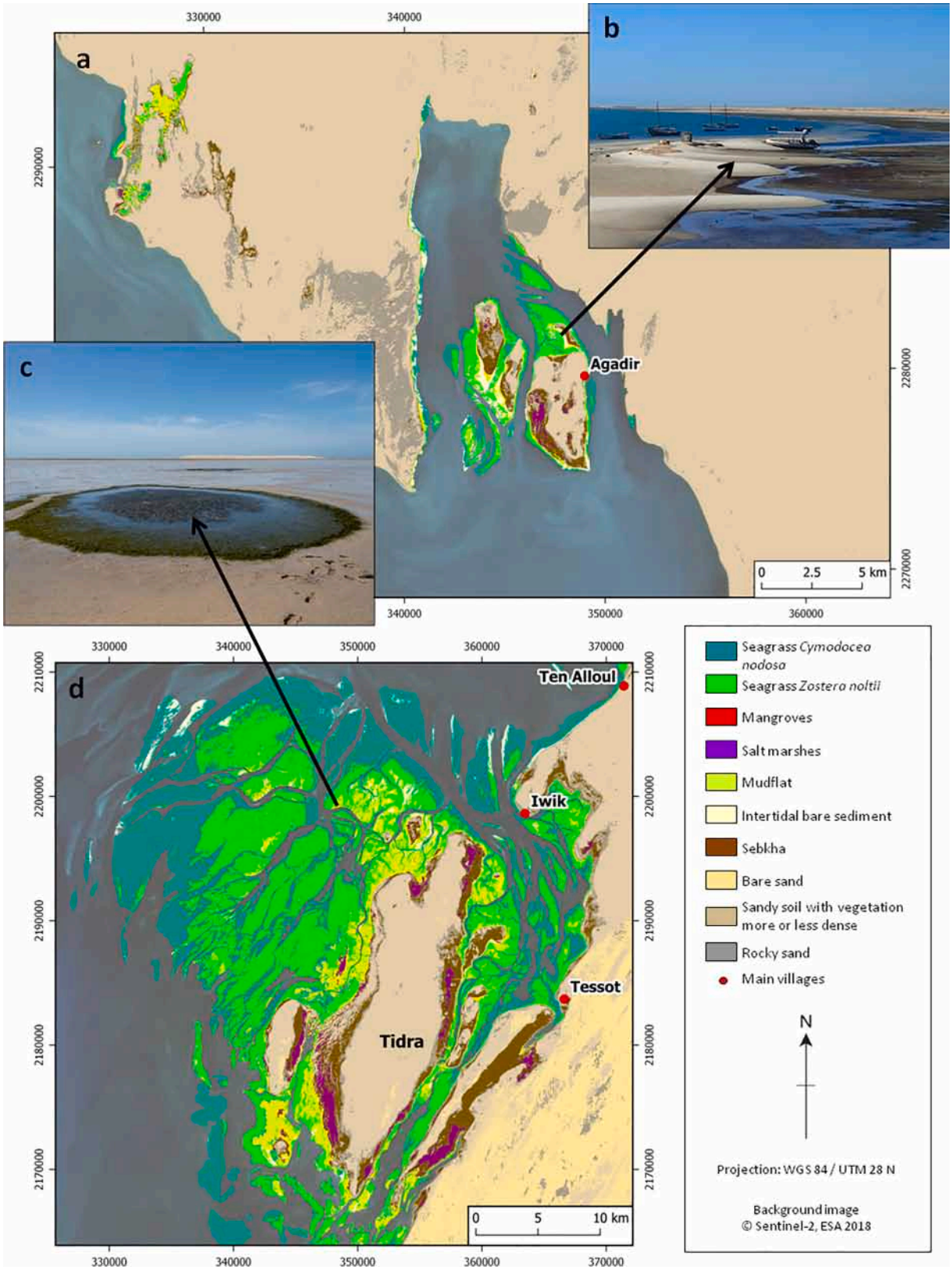


**Fig. 6.** Mapping of marine and terrestrial biocenosis of the northern and central part of the PNBA using Sentinel-2 imagery. a- northern part (Agadir), b- seagrass partly submerged near sandbanks, c- Cymodocea seagrass in small intertidal ponds, d- central part (Tidra island and surroundings).

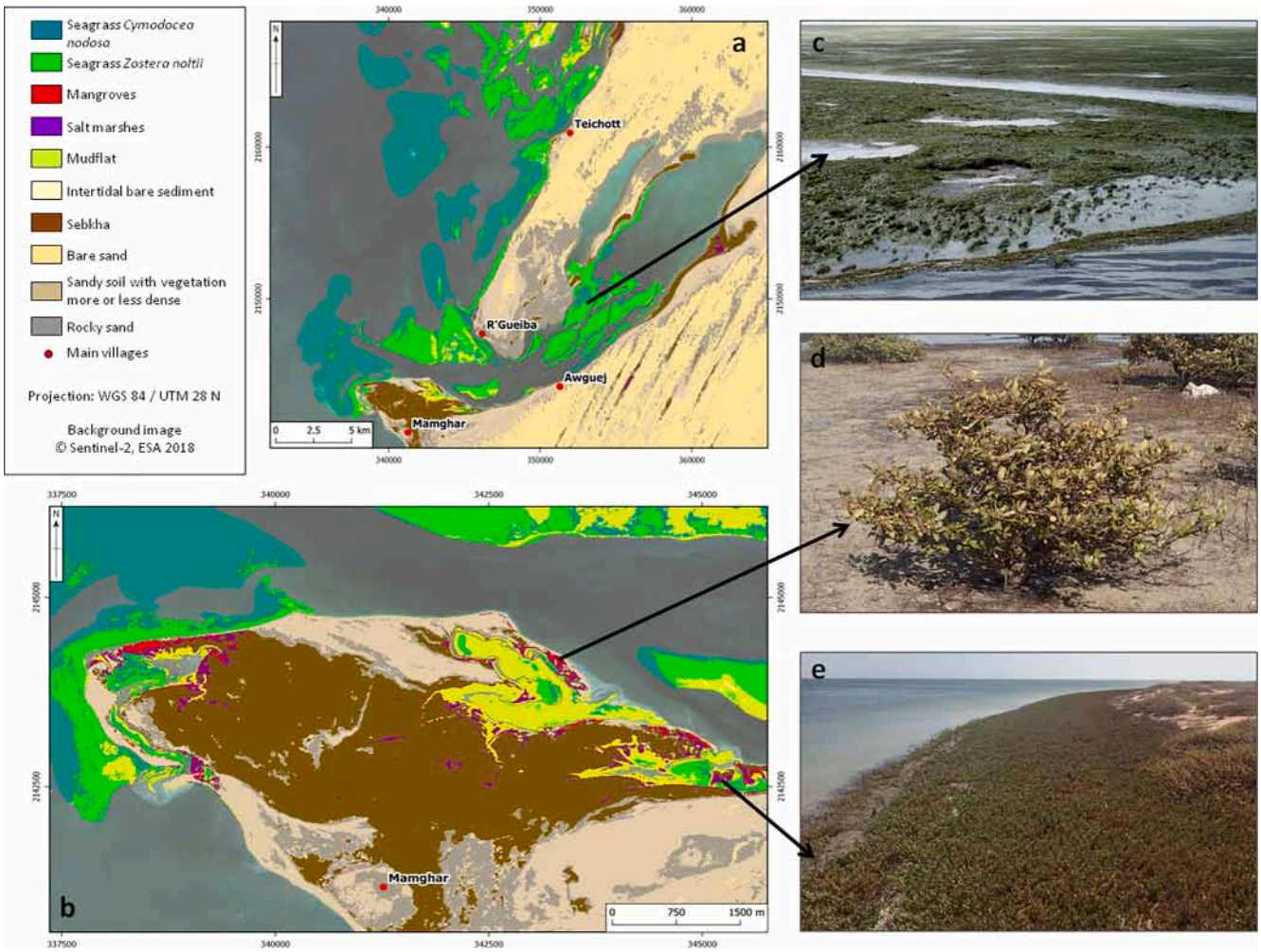


**Fig. 7.** Mapping of marine and terrestrial biocenosis of the southern part of the PNBA using Sentinel-2 data. a- overview of the southern part, b- detail of the southern-west extremity of the park (near Mamghar) where small patches of mangroves are located, c- *Zostera noltii* beds with partly emerged Cymodocea, d- mangroves (*Avicennia germinans*), e- salt marshes.

**Table 3**
Detailed confusion matrix for 02/22/2018. Class 1*: Seagrass without distinction; Class 1: Seagrass *Cymodocea*; Class 2: Seagrass *Zostera*; Class 3: Mangroves; Class 4: Salt marshes; Class 5: Mudflat; Class 6; Intertidal bare sediment; Class 7: Sebkha.

| | 1* | 1 | 2 | 3 | 4 | 5 | 6 | 7 | Total |
|---|---|---|---|---|---|---|---|---|---|
| **1*** | **77** | – | – | 0 | 0 | 0 | 0 | 0 | 77 |
| **1** | – | **26** | 14 | 0 | 0 | 0 | 0 | 0 | 40 |
| **2** | – | 13 | **24** | 0 | 0 | 0 | 0 | 0 | 37 |
| **3** | 1 | 0 | 1 | **7** | 12 | 1 | 0 | 0 | 22 |
| **4** | 0 | 0 | 0 | 0 | **23** | 1 | 0 | 1 | 25 |
| **5** | 1 | 0 | 1 | 0 | 0 | **12** | 2 | 0 | 15 |
| **6** | 2 | 0 | 2 | 0 | 0 | 0 | **11** | 0 | 13 |
| **7** | 0 | 0 | 0 | 0 | 0 | 0 | 1 | **23** | 24 |
| **Total** | 81 | 39 | 42 | 7 | 36 | 14 | 14 | 24 | 176 |
| **Class specific precision (%)** | **95** | **66.7** | **58.5** | **100** | **61** | **85.7** | **78.6** | **82** | – |
| **Class specific recall** | **1** | **0.65** | **0.64** | **0.32** | **0.8** | **0.8** | **0.85** | **0.96** | – |
| **F-score** | **0.97** | **0.66** | **0.61** | **0.48** | **0.69** | **0.83** | **0.81** | **0.88** | – |
| **Overall accuracy** | – | – | – | – | – | – | – | – | – |
| with distinction of seagrass | – | – | – | – | – | – | – | – | **71.6** |
| without distinction of seagrass | – | – | – | – | – | – | – | – | **86.7** |
| **Kappa index** | – | – | – | – | – | – | – | – | – |
| with distinction of seagrass | – | – | – | – | – | – | – | – | **0.66** |
| without distinction of seagrass | – | – | – | – | – | – | – | – | **0.8** |

moderate accuracy of 61%, which gives us an F-score of 0.69. It means that the classification identified a lot of true salt marsh pixels, but also false salt marsh pixels, hence the overdetection of salt-marsh.

For mudflats and bare intertidal sediments, we obtained an accuracy of 85.7% and 78.6%, a recall of 0.8 and 0.85 and an F-score of 0.83 and 0.81, respectively. We can notice some confusion between mudflats and

**Table 4**
Summary of the confusion matrices of the 5 classifications on the marine part (distinguished seagrass).

| | 12/09/2017 | 12/24/2017 | 01/08/2018 | 02/22/2018 | 02/27/2018 |
|---|---|---|---|---|---|
| **Seagrass *Cymodocea* (1)** | 57.4 | 56.7 | 54.4 | 66.7 | 58.3 |
| **Seagrass *Zostera* Noltii (2)** | 55.6 | 60 | 52.4 | 58.5 | 57.1 |
| **Mudflat (5)** | 90 | 90 | 86.7 | 100 | 100 |
| **Intertidal bare sediment (6)** | 76.9 | 71.4 | 90.9 | 83.3 | 66.7 |
| **Overall accuracy** | 62.5 | 62.5 | 62.5 | 69.2 | 62.5 |
| **Kappa index** | 0.448238 | 0.448763 | 0.45204 | 0.55118 | 0.447336 |

**Table 5**
Summary of the confusion matrices of the 5 classifications on the marine part (seagrass merged).

| | 12/09/2017 | 12/24/2017 | 01/08/2018 | 02/22/2018 | 02/27/2018 |
|---|---|---|---|---|---|
| **Seagrass without distinction (1*)** | 93.8 | 95 | 96.2 | 98.1 | 95.1 |
| **Mudflat (5)** | 90 | 90 | 86.7 | 100 | 100 |
| **Intertidal bare sediment (6)** | 76.9 | 71.4 | 90.9 | 83.3 | 66.7 |
| **Overall accuracy** | 91.3 | 91.3 | 94.2 | 95.2 | 91.3 |
| **Kappa index** | 0.78095 | 0.784232 | 0.85987 | 0.879963 | 0.781257 |

bare intertidal sediments, which can be explained by their close nature (radiometrically), but also with seagrass beds. Finally, sebkha obtained 82% accuracy, 0.96 recall and 0.88F-score which is a good result.

For the 4 other classifications (12/09/2017, 12/24/2017, 01/08/2017 and 02/27/2018) on the maritime part with seagrass *Cymodocea* and *Zostera* separated, we obtained similar results between the classification of the 22 February 2018 and the other classifications (detailed confusion matrices can be found in the supplementary material). Indeed, we observed same confusions between intra-class classification of seagrass with respectively 57.4%, 56.7%, 54.4%, 66.7% and 58.3% of accuracy for *Cymodocea* seagrasss and 55.6%, 60%, 52.4%, 58.5% and 57.1% for *Zostera* seagrass (Table 4). As for the recall and F-score, we obtained respectively between 0.65 and 0.86 of recall with an average of 0.78 and between 0.6 and 0.7 with an average of 0.66 for F-score for the class seagrass *Cymodocea* and between 0.3 and 0.6 of recall with an average of 4 and between 0.38 and 0.62 with an average of 0.46 for F-score for the class seagrass *Zostera* (Supplementary data 1–5). We also found the same confusion between mudflat and intertidal bare sediment with respectively 90%, 90%, 86.7%, 100% and 100% accuracy for mudflat and 76.9%, 71.4%, 90.9%, 83.3% and 66.7% for intertidal bare sediment. Besides, statistics results were similar if we compared classifications with seagrass merged into one single class (Table 5). Thus, these results show that our method is robust to map seagrass since we obtained similar statistics results at different dates, though the intra-class detection should be taken with caution since spectral discrimination of seagrass at species level using multispectral sensor is pratically impossible.

### 5.2. Extent of the ecosystems

For Sentinel-2 in 2018, the calculated extents are closed to the ones obtained in the PACOBA project from 2003 imagery (total seagrass surface of 772 $km^2$). We detected 353 $km^2$ of *Zostera* seagrass, which is 100 $km^2$ less than the surface detected in 2003 with the SPOT-5 image, and 419 $km^2$ of *Cymodocea* seagrass, compared to the reference value of 374 $km^2$, which is around 45 $km^2$ more than the previous result. Thus, we detected a total of 772 $km^2$ of seagrass, which is almost the same as the reference (774 $km^2$). Our results highlight a very high overall stability of this ecosystem, despite the high spatial variability of its distribution over time (Fig. 8). The detection difference between the surfaces is explained by the strong spectral similarity between Zostera and Cymodocea causing misclassifications. For mangroves, the detected surface in 2018 were lower than the reference due to the change in spatial image resolution from SPOT-5 (2.5 m) to Sentinel-2 (10 m), combined to the small size of mangrove patches. Finally, we detected slightly less mudflat coverage than the reference, due to misclassification with bare intertidal sediments, which has a similar spectral response.

### 5.3. Seagrass density estimation from Sentinel-2 imagery

During the field acquisition in April 2018, we collected data on seagrass density (Low, Mean, High). Next, we attempted to use these data to extrapolate the density of seagrass beds based on the Sentinel-2 radiometry. The results are very unsatisfactory because only 20% of measured densities agree with densities extracted from radiometry. The low accuracy might result from the 10-m resolution of Sentinel-2, as estimated densities were averaged over 100 $m^2$ areas, while densities on the field were probably representative of a smaller area. Fig. 9 introduces a map of seagrass densities from the spectral signal around Tidra island, with three classes: high density, medium density, and low density for *Zostera noltii* and *Cymodocea nodosa*.

### 5.4. Insights from the 1.5 m resolution data

In the frame of this study, we were able to access a limited amount of very high-resolution archive data from SPOT-6 satellite in the northern part of Mamghar, where the majority of mangrove forests are present in the park, provided freely by EQUIPEX GEOSUD (http://ids.equipex-geosud.fr) and dated January 24th, 2016 (no data were available for 2018 on the study area). The data, at 1.5 m resolution, were already preprocessed (*ortho*-rectification and pan-sharpening) by GEOSUD and were composed of 4 bands (Red, Green, Blue, and Near Infrared). We found that Sentinel-2 high-resolution was likely to over-estimate the extent of mangroves in the PNBA due to a large number of mixed pixels classified as mangroves. The SPOT-6 very high resolution allowed a fine detection of mangroves, even small objects, which is more suitable in the PNBA, given the patchy and scarce distribution of mangroves (Fig. 10). However, besides being “freely available” data, the use of SPOT-6 data requires important resources in terms of processing power, calculation time and storage. Therefore, a very high resolution should be used for small study areas or local applications, while high spatial resolution such as Sentinel-2 is more suitable for larger areas, like the PNBA.

## 6. Applications of the mapping of marine coastal ecosystems in the PNBA

The mapping of marine ecosystems of the PNBA using Sentinel-2 provides up-to-date knowledge on their distribution and extent. We showed that Sentinel 2 has a strong potential for this matter thanks to the temporal repetitivity that allows access to high quality imagery (maximum water quality), free of charge, on large areas. Many algorithms are available to preprocess coastal waters and map water quality using Sentinel 2. The reproducibility of our supervised approach is very dependent on the availability of field data availability and quality for the training of the algorithm and validation. This is a limitation than can be overcome using available products provided by ESA for instance. Such mapping is an essential prerequisite for the assessment of ecosystem services in the PNBA (Trégarot et al. 2018).

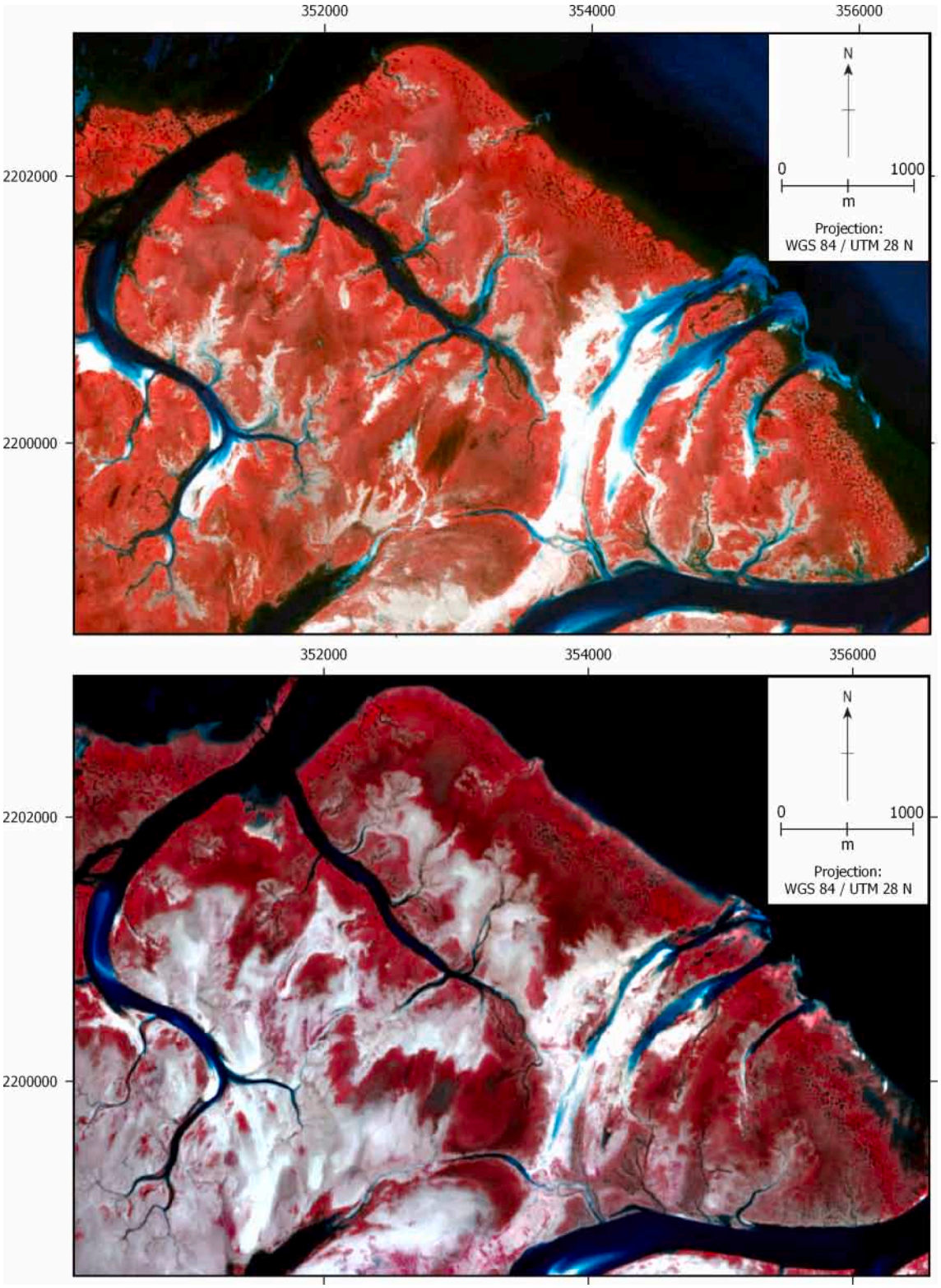


**Fig. 8.** Spatio-temporal variations in the distribution of the seagrass in an area of the PNBA, comparison between a 2003 SPOT-5 image in false colour infra-red (Top, © CNES – 2003, Distribution Airbus DS, all rights reserved) and a 2018 Sentinel-2 image in false color(Bottom, ©ESA, 2018). (For interpretation of the references to color in this figure legend, the reader is referred to the web version of this article.)

Seagrass stores 10–15% of the ocean organic carbon (Duarte et al., 2004; Kennedy and Björk, 2009), and are considered as autotrophic ecosystems acting as carbon sinks (Lavery et al. 2013). Indeed, the estimated net productivity of seagrass beds is 1.19 t C/ha/year, equivalent to 435 t $CO^2$eq/$km^2$/year on average (Duarte et al., 2010; Trégarot et al., 2017). Seagrass biomass and the sedimentary substrate are both involved in the storage of carbon, but their degradation can also act as a source of carbon (Pendleton et al. 2012).

Recent studies by Gullström et al. (2018) showed that the capability of seagrass to store carbon is dependent on the species, the type of

**Table 6**
Surface areas (km$^2$) and percentage of surface detected on coastal marine ecosystems in the PNBA from Sentinel-2 imagery in February 2018.

| Classes | Area (km$^2$) | % surface |
|---|---|---|
| Seagrass *Cymodocea nodosa* | 419 | 40 |
| Seagrass *Zostera noltii* | 353 | 34 |
| **Total Seagrass** | 772 | 74 |
| Mangroves | 0.5 | 0.05 |
| Salt marshes | 23 | 2 |
| Mudflats | 98 | 9 |
| Intertidal bare sediment | 21 | 2 |
| Sebkha | 123 | 12 |
| **Total** | 1037 | 100 |

sediments, and the connectivity with adjacent ecosystems, highlighting the importance in mapping seagrass beds and associated ecosystems. Although the assessment of carbon storage potential in the marine ecosystems of the PNBA is limited by the availability of data, the extent of seagrass beds in the area (74% of mapped surfaces), makes them the most important component of carbon storage in the PNBA, compared to other ecosystems whose relative coverage reach 12% for sebkha, 9% for mudflats, 2% for salt marshes and 0.05% for mangroves. Mudflats might play a major role in the carbon storage thanks to the presence of microphytobenthos (Barnett, 2013), although we were not able to map the distribution of microphytobenthos density. Our results provide new elements on the global coverage of marine ecosystems in the PNBA. Complementary studies have to be carried out to quantify precisely carbon storage in the PNBA.

The PNBA contains 772 km$^2$ of seagrass, with 419 km$^2$ of subtidal *Cymodocea nodosa* and 353 km$^2$ of intertidal *Zostera noltii*. Their capability to mitigate wave and current energy depends on the water level and the amount of vegetation in the water column, along with morphological characteristics of plants such as the rigidity, density, length and morphology of the leaves (Fonseca and Cahalan, 1992; Koch et al., 2006; Ward et al., 1984). In the PNBA, both species locally reach high densities and occupy a large part of the water column combining two important properties for coastal protection. The service of coastal protection is pressing in the context of climate change for low elevated dwellings as found in the PNBA. The mapping of coastal marine habitats, combined with the capacity of ecosystems to attenuate wave and current energy could highlight priority areas for conservation where environmental and socio-economic stakes are at risk of sea-level rise and flooding.

The canopy of seagrass beds in the PNBA also allows juveniles of fish and invertebrates to find refuge against predators (Dewsbury et al., 2016; Jackson et al., 2015; Schaffmeister et al., 2006). The Banc d'Arguin is likely an important nursery area for commercial fish and shrimps who use seagrass beds for refuge against predators (Gushchin and Fall, 2012; Jager, 1993; Schaffmeister et al., 2006; van Etten, 2003). The function of nursery is essential to maintain adult population targeted by artisanal and commercial fisheries in the PNBA and outside the Park. Even the intertidal flats, that are covered by ponds (van der Laan and Wolff, 2006), provide a substantial function of nursery, particularly for shrimps (Schaffmeister et al., 2006). Although not visible on the maps using Sentinel-2 data, we showed that very high resolution SPOT 6 data could provide information on ecosystems distributed in small patches. Such data could also help identify intertidal ponds in the PNBA.

Seagrass provide essential services to human communities. For instance, commercial fish or shrimp juveniles of some species can use intertidal ponds within seagrass as nurseries, refuge against predators (Dewsbury et al., 2016; Jackson et al., 2015; Schaffmeister et al., 2006). These ponds also reduce intra-specific competition for the resource (Heck et al., 2003). Although not visible on the maps using Sentinel-2 data, we showed that very high resolution SPOT 6 data can provide

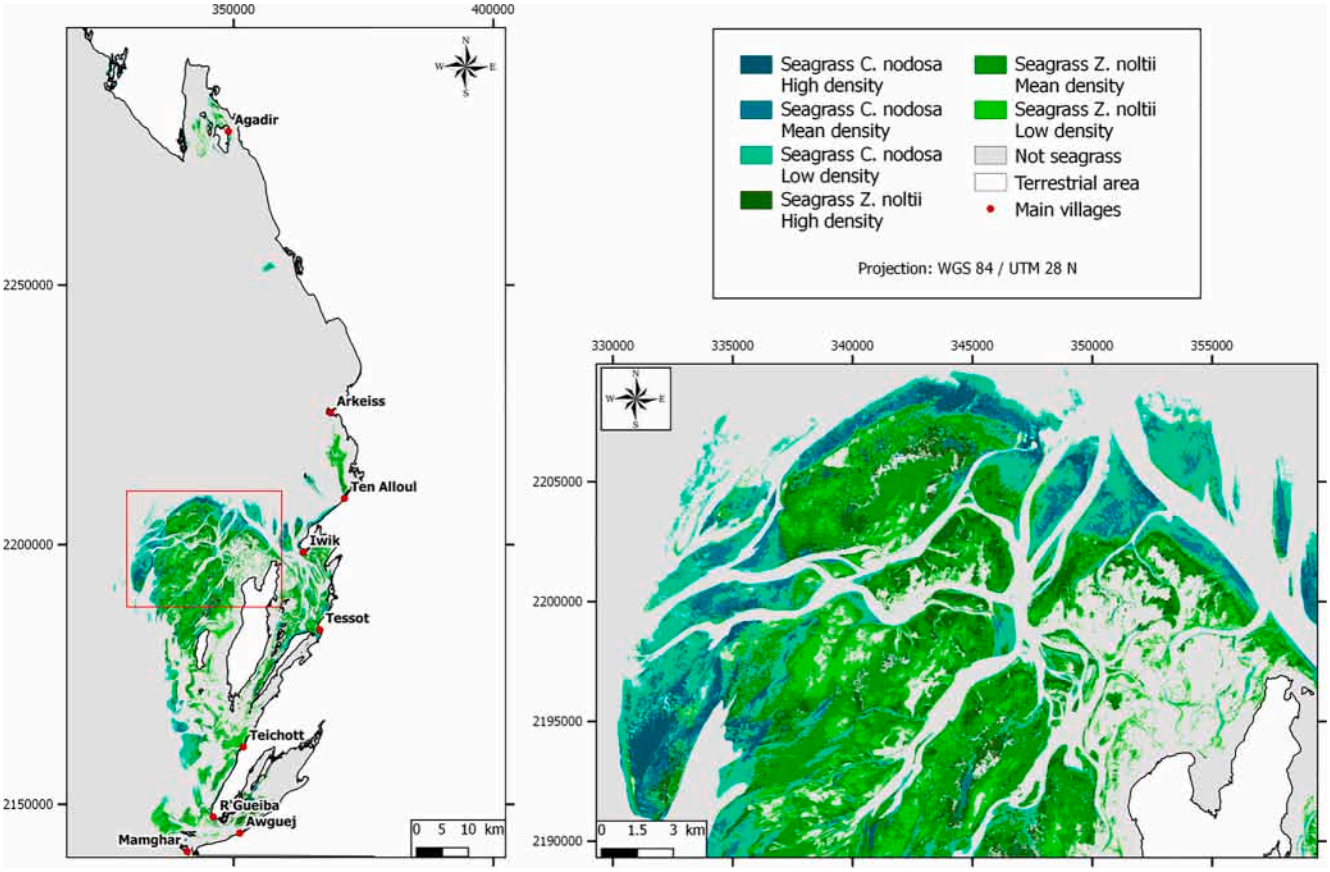


**Fig. 9.** Map of seagrass densities for *Zostera noltii* and *Cymodocea nodosa* in northern Tidra island (right panel), National Park of Banc d'Arguin, Mauritania.

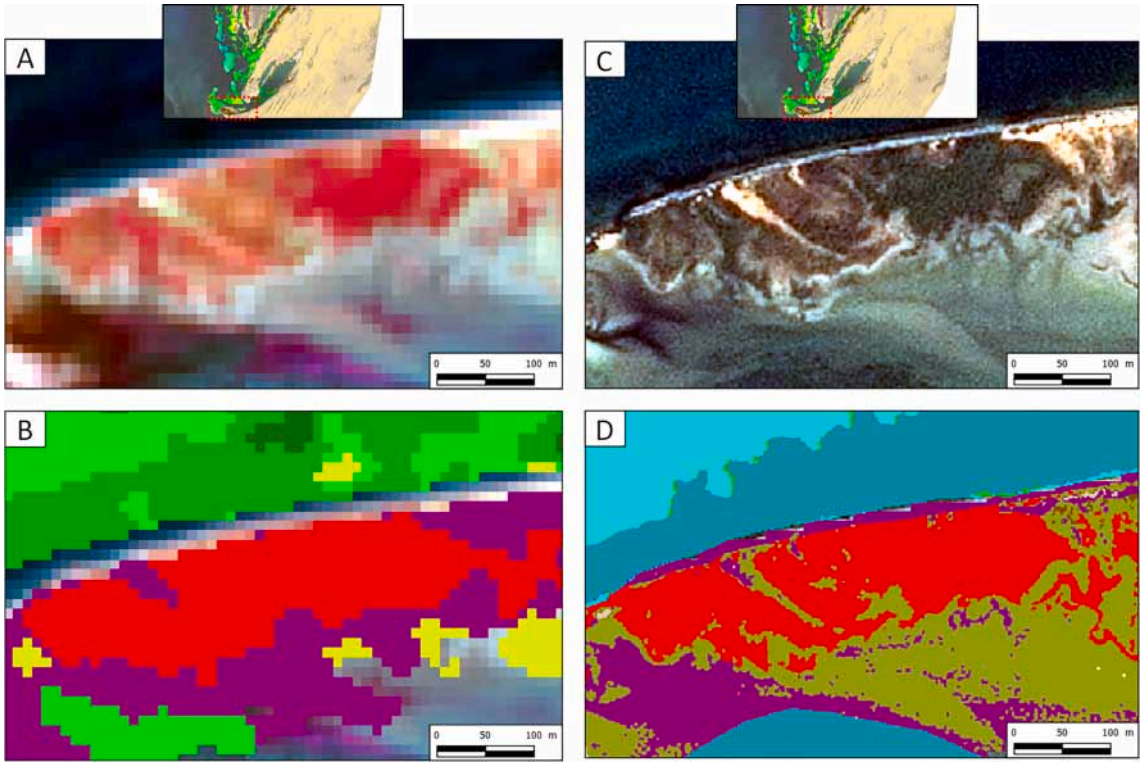


**Fig. 10.** Comparison of mangroves' detection (in red) between Sentinel-2 (A and B) and SPOT-6 (C and D) in the northern part of Mamghar, National Park of Banc d'Arguin, Mauritania. (For interpretation of the references to color in this figure legend, the reader is referred to the web version of this article.)

information on ecosystems distributed in small patches. Such data can also help identify intertidal ponds in the PNBA.

## 7. Conclusion

This study updated ecosystem knowledge and maps of the marine and terrestrial ecosystems of the PNBA using Sentinel-2 data of 10 m resolution. Our results showed this sensor is an adequate tool to map the extent of marine ecosystems at a large scale. The wide swath of Sentinel-2 is very suitable for a global mapping approach, and its high temporal resolution ensures free regular updates for many years via the European Space Agency (ESA) Copernicus programme. Preprocessing and processing were developed entirely on open-source software and the methodology can easily be transferred to local actors for future updates of the maps.

Our study provides the first seagrass mapping throughout the entire area of the PNBA, especially in the northern part that was not well-known so far. Our approach provides a method for the implementation of seagrass extent surveying in the PNBA. Given the strong variability of its distribution in time and space and its vulnerability towards natural and anthropic pressures, it is extremely relevant for conservation actions in this protected area. The dynamics of seagrass are also closely related to the dynamics of other ecosystems in the park, that is why we considered the whole marine ecosystems in this study. Further research on the PNBA should focus on (i) making such monitoring tool operational for local actors of conservation, (ii) the integration of other data such as bathymetry, coastal and benthic habitat maps provided by agencies like ESA, (iii) and the interactions between human, animal species and marine ecosystems to better assess ecosystem services and reinforce conservation actions of the protected are of the PNBA.

## CRediT authorship contribution statement

**A. Pottier:** Conceptualization, Data curation, Formal analysis, Investigation, Methodology, Software, Writing - original draft, Writing - review & editing. **T. Catry:** Conceptualization, Data curation, Formal analysis, Investigation, Methodology, Writing - original draft, Writing - review & editing. **E. Trégarot:** Conceptualization, Investigation, Methodology, Project administration, Writing - review & editing. **J.-P. Maréchal:** Data curation, Investigation. **V. Fayad:** Data curation, Investigation. **G. David:** Conceptualization, Investigation. **M. Sidi Cheikh:** Conceptualization, Investigation, Validation. **P. Failler:** Conceptualization, Funding acquisition, Investigation, Project administration, Supervision, Writing - review & editing.

## Declaration of Competing Interest

The authors declare that they have no known competing financial interests or personal relationships that could have appeared to influence the work reported in this paper.

*Acknowledgements*

This study was financially supported by public funds received in the framework of GEOSUD, a project (ANR-10-EQPX-20) of the program "Investissements d'Avenir" managed by the French National Research Agency (ANR), and by the French Development Agency (AFD), the French Facility for Global Environment (FFEM) and the Trust-Fund for the Banc d'Arguin and the Coastal & Marine Biodiversity (BACOMAB). We thank Jean-Claude Lorente from Centre de coopération internationale en recherche agronomique pour le développement (CIRAD) for the assistance with the map designing and realization.

*Software*

QGIS, ACOLITE processor, Orfeo Toolbox and R Studio were used in this study.

## Appendix A. Supplementary material

Supplementary data to this article can be found online at https://doi.org/10.1016/j.jag.2021.102419.

## References


Al-Kharusi, E.S., Tenenbaum, D.E., Abdi, A.M., Kutser, T., Karlsson, J., Bergström, A.K., Berggren, M., 2020. Large-scale retrieval of coloured dissolved organic matter in northern lakes using Sentinel-2 data. Remote Sens. 12 (1), 157.

Bakirman, T., Gumusay, M.U., Tuneyb, I., 2016. Mapping of the seagrass cover along the Mediterranean coast of Turkey using Landsat 8 OLI images. Int. Arch. Photogramm., Remote Sens. Spatial Inform. Sci. 8.

Barbier, E.B., Hacker, S.D., Kennedy, C., Koch, E.W., Stier, A.C., Silliman, B.R., 2011. The value of estuarine and coastal ecosystem services. Ecol. Monogr. 81 (2), 169–193.

Barnett, A., 2013. Regulation of photosynthetic activity of microphytobenthos and consequence on the temporal dynamics of primary production in intertidal mudflats on the Atlantic coast of Western Europe. Ph.D. thesis. University of La Rochelle, p. 360.

Bramich, J., Bolch, C.J., Fischer, A., 2021. Improved red-edge chlorophyll-a detection for Sentinel 2. Ecol. Ind. 120, 106876.

Caballero, I., Stumpf, R.P., 2020. Towards routine mapping of shallow bathymetry in environments with variable turbidity: contribution of Sentinel-2A/B satellites mission. Remote Sensing 12 (3), 451.

Chen, S.N., Sanford, L.P., Koch, E.W., Shi, F., North, E.W., 2007. A nearshore model to investigate the effects of seagrass bed geometry on wave attenuation and suspended sediment transport. Estuaries Coasts 30 (2), 296–310.

Cohen, J. (1960). A coefficient of agreement for nominal scales. Ed. Psychol. Measure. 20 (1), 37-46.

Coll, M., Piroddi, C., Steenbeek, J., Kaschner, K., Lasram, F. B. R., Aguzzi, J., et al., 2010. The biodiversity of the Mediterranean Sea: estimates, patterns, and threats. PloS one, 5(8), e11842.

Congalton, R.G., 1991. A review of assessing the accuracy of classifications of remotely sensed data. Remote Sens. Environ. 37 (1), 35–46.

Congalton, R.G., Green, K., 1999. Assessing the accuracy of remotely sensed data: Principles and practices. Lewis Publishers, Boca Raton.

Dekker, A., Brando, V., Anstee, J., Fyfe, S., Malthus, T., Karpouzli, E., 2007. Remote sensing of seagrass ecosystems: Use of spaceborne and airborne sensors. In Seagrasses: Biology, Ecologyand Conservation (pp. 347-359). Springer, Dordrecht.

De la Torre-Castro, M.D., Rönnbäck, P., 2004. Links between humans and seagrasses—an example from tropical East Africa. Ocean Coast. Manag. 47 (7–8), 361–387.

Demarcq, H., Faure, V., 2000. Coastal upwelling and associated retention indices derived from satellite SST. Application to Octopus vulgaris recruitment. Oceanol. Acta 23 (4), 391–408.

Dewsbury, B.M., Bhat, M., Fourqurean, J.W., 2016. A review of seagrass economic valuations: gaps and progress in valuation approaches. Ecosyst. Serv. 18, 68–77.

Dobson, J. E. (1995). NOAA Coastal Change Analysis Program (C-CAP): guidance for regional implementation.

Duarte, C.M., 1990. Seagrass nutrient content. Marine Ecol. Prog. Ser. Oldendorf 6 (2), 201–207.

Duarte, C.M., 2002. The future of seagrass meadows. Environ. Conserv. 29 (2), 192–206.

Duarte, C.M., Middelburg, J.J., Caraco, N., 2004. Major role of marine vegetation on the oceanic carbon cycle. Biogeosci. Discuss. 1 (1), 659–679.

Duarte, C.M., Marbà, N., Gacia, E., Fourqurean, J.W., Beggins, J., Barrón, C., Apostolaki, E.T., 2010. Seagrass community metabolism: Assessing the carbon sink capacity of seagrass meadows. Global Biogeochem. Cycles 24 (4).

Eugenio, F., Marcello, J., Martin, J., 2015. High-resolution maps of bathymetry and benthic habitats in shallow-water environments using multispectral remote sensing imagery. IEEE Trans. Geosci. Remote Sens. 53 (7), 3539–3549.

Evrard, V., Kiswara, W., Bouma, T.J., Middelburg, J.J., 2005. Nutrient dynamics of seagrass ecosystems: 15N evidence for the importance of particulate organic matter and root systems. Mar. Ecol. Prog. Ser. 295, 49–55.

Ferguson, R.L., Wood, L.L., Graham, D.B., 1993. Monitoring spatial change in seagrass habitat with aerial photography. Photogramm. Eng. Remote Sens. 59 (6).

Fonseca, M.S., Cahalan, J.A., 1992. A preliminary evaluation of wave attenuation by four species of seagrass. Estuar. Coast. Shelf Sci. 35, 565–576.

Foody, G.M., Mathur, A., 2004a. A relative evaluation of multiclass image classification by support vector machines. IEEE Trans. Geosci. Remote Sens. 42 (6), 1335–1343.

Foody, G.M., Mathur, A., 2004b. Toward intelligent training of supervised image classifications: directing training data acquisition for SVM classification. Remote Sens. Environ. 93 (1–2), 107–117.

Fourqurean, J.W., Duarte, C.M., Kennedy, H., Marbà, N., Holmer, M., Mateo, M.A., et al., 2012. Seagrass ecosystems as a globally significant carbon stock. Nat. Geosci. 5 (7), 505.

Frigge, M., Hoaglin, D.C., Iglewicz, B., 1989. Some implementations of the boxplot. Am. Statist. 43 (1), 50–54.

Green, E.P., Mumby, P.J., Edwards, A.J., Clark, C.D., 1996. A review of remote sensing for the assessment and management of tropical coastal resources. Coast. Manage. 24 (1), 1–40.

Gullström, M., Lyimo, L.D., Dahl, M., Samuelsson, G.S., Eggertsen, M., Anderberg, E., Rasmusson, L.M., Linderholm, H.W., Knudby, A., Bandeira, S., Nordlund, L.M., 2018. Blue carbon storage in tropical seagrass meadows relates to carbonate stock dynamics, plant–sediment processes, and landscape context: insights from the western Indian Ocean. Ecosystems 21, 551–566.

Guénette, S., Meissa, B., Gascuel, D., 2014. Assessing the contribution of marine protected areas to the trophic functioning of ecosystems: a model for the Banc d'Arguin and the Mauritanian shelf. PLoS ONE 9 (4), e94742.

Gushchin, A., Fall, K.O.M., 2012. Ichthyofauna of littoral of the gulf Arguin, Mauritania. J. Ichthyol. 52, 160–171.

Heck Jr, K., Hays, G., Orth, R.J., 2003. Critical evaluation of the nursery role hypothesisfor seagrass meadows. Mar. Ecol. Prog. Ser. 123–136.

Hossain, M.S., Bujang, J.S., Zakaria, M.H., Hashim, M., 2015. The application of remote sensing to seagrass ecosystems: an overview and future research prospects. Int. J. Remote Sens. 36 (1), 61–114.

Hossain, M.S., Hashim, M., 2019. Potential of Earth Observation (EO) technologies for seagrass ecosystem service assessments. Int. J. Appl. Earth Obs. Geoinf. 77, 15–29.

Huang, C., Davis, L.S., Townshend, J.R.G., 2002. An assessment of support vector machines for land cover classification. Int. J. Remote Sens. 23 (4), 725–749.

Jackson, E.L., Rees, S.E., Wilding, C., Attrill, M.J., 2015. Use of a seagrass residency index to apportion commercial fishery landing values and recreation fisheries expenditure to seagrass habitat service. Conserv. Biol. 29, 899–909.

Jager, Z., 1993. The distribution and abundance of young fish in the Banc d'Arguin, Mauritania. Hydrobiologia 258, 185–196.

Kovacs, E., Roelfsema, C., Lyons, M., Zhao, S., Phinn, S., 2018. Seagrass habitat mapping: how do Landsat 8 OLI, Sentinel-2, ZY-3A, and Worldview-3 perform? Remote Sens. Lett. 9 (7), 686–695.

Kendrick, G.A., Aylward, M.J., Hegge, B.J., Cambridge, M.L., Hillman, K., Wyllie, A., Lord, D.A., 2002. Changes in seagrass coverage in Cockburn Sound, Western Australia between 1967 and 1999. Aquat. Bot. 73 (1), 75–87.

Kennedy H. et Björk M. (2009). Seagrass meadows. In: Laffoley, D. et Grimsditch, G. (Eds). The management of natural coastal carbon sinks, IUCN, Gland, Switzerland. 53 p.

Kennedy, H., Beggins, J., Duarte, C.M., Fourqurean, J.W., Holmer, M., Marbà, N., Middelburg, J.J., 2010. Seagrass sediments as a global carbon sink: isotopic constraints. Global Biogeochem. Cycles 24 (4).

Kirkman, H., 1996. Baseline and monitoring methods for seagrass meadows. J. Environ. Manage. 47 (2), 191–201.

Koch, E. W., Sanford, L. P., Chen, S.-N., Shafer, D. J. et Smith, J. M. (2006). Waves in seagrass systems: review and technical recommendations. Maryland University, Cambridge Center for Environmental Science.

Kutser, T., Dekker, A. G., Skirving, W., 2003. Modeling spectral discrimination of Great Barrier Reef benthic communities by remote sensing instruments. Limnol. Oceanogr., 48(1part2), 497-510.

Kutser, T., Vahtmäe, E., Metsamaa, L. (2006). Spectral library of macroalgae and benthic substrates in Estonian coastal waters. Proc. Estonian Acad. Sci. Biol. Ecol, 55(4), 329-340.

Kutser, T., Hedley, J., Giardino, C., Roelfsema, C., Brando, V.E., 2020. Remote sensing of shallow waters–a 50 year retrospective and future directions. Remote Sens. Environ. 240, 111619.

Landis, J.R., Koch, G.G., 1977. The measurement of observer agreement for categorical data. Biometrics 159–174.

Lavery, P.S., Mateo, M.Á., Serrano, O., Rozaimi, M., 2013. Variability in the carbon storage of seagrass habitats and its implications for global estimates of blue carbon ecosystem service. PLoS ONE 8 (9), e73748.

Lebigre, J.M., 1991. Les marais maritimes de Mauritanie: Protection et valorisation. Les cahiers d'outre-mer 44 (176), 379–400.

Lee, Z., Carder, K.L., 2002. Effect of spectral band numbers on the retrieval of water column and bottom properties from ocean color data. Appl. Opt. 41 (12), 2191–2201.

Lyons, M.B., Roelfsema, C.M., Phinn, S.R., 2013. Towards understanding temporal and spatial dynamics of seagrass landscapes using time-series remote sensing. Estuar. Coast. Shelf Sci. 120, 42–53.

Lyons, M., Phinn, S., Roelfsema, C., 2011. Integrating Quickbird multi-spectral satellite and field data: mapping bathymetry, seagrass cover, seagrass species and change in Moreton Bay, Australia in 2004 and 2007. Remote Sensing 3 (1), 42–64.

Matta, E., Aiello, M., Bresciani, M., Gianinetto, M., Musanti, M., Giardino, C., 2014, July. Mapping Posidonia meadow from high spatial resolution images in the Gulf of Oristano (Italy). In 2014 IEEE Geoscience and Remote Sensing Symposium (pp. 5152-5155). IEEE.

McFeeters, S.K., 1996. The use of the Normalized Difference Water Index (NDWI) in the delineation of open water features. Int. J. Remote Sens. 17 (7), 1425–1432.

McKenzie, L.J., Finkbeiner, M.A., Kirkman, H., 2001. Methods for mapping seagrass distribution. Global Seagrass Res. Methods 101–121.

McKenzie, L.J., Yoshida, R.L., 2020. Over a decade monitoring Fiji's seagrass condition demonstrates resilience to anthropogenic pressures and extreme climate events. Mar. Pollut. Bull. 160, 111636.

Mountrakis, G., Im, J., Ogole, C., 2011. Support vector machines in remote sensing: A review. ISPRS J. Photogramm. Remote Sens. 66 (3), 247–259.

Nagelkerken, I., Roberts, C.V., Van Der Velde, G., Dorenbosch, M., Van Riel, M.C., De La Moriniere, E.C., Nienhuis, P.H., 2002. How important are mangroves and seagrass beds for coral-reef fish? The nursery hypothesis tested on an island scale. Mar. Ecol. Prog. Ser. 244, 299–305.

Ondiviela, B., Losada, I.J., Lara, J.L., Maza, M., Galván, C., Bouma, T.J., van Belzen, J., 2014. The role of seagrasses in coastal protection in a changing climate. Coast. Eng. 87, 158–168.

Orth, R.J., Carruthers, T.J., Dennison, W.C., Duarte, C.M., Fourqurean, J.W., Heck, K.L., et al., 2006. A global crisis for seagrass ecosystems. Bioscience 56 (12), 987–996.

Ould Cheikh, A. W., 2002a. L'Identité imraguen et la gestion locale de l'aire du PNBA: approche historique et sociologique. Nouakchott, Parc national du banc d'Arguin.

Ould Cheikh, A.W., 2002b. Création, évolution, peuplement et identité imraguen, gestion de l'espace. Le Parc national du Banc d'Arguin, Nouakchott, CONSDEV.
Paringit, E. C., Nadaoka, K., Fortes, M. D., Harii, S., Tamura, H., Mitsui, J., Strachan, J. J., 2003, July. Multiangular and hyperspectral reflectance modeling of seagrass beds for remote sensing studies. In IGARSS 2003. 2003 IEEE International Geoscience and Remote Sensing Symposium. Proceedings (IEEE Cat. No. 03CH37477) (Vol. 3, pp. 2128-2130). IEEE.
Pereira-Sandoval, M., Ruescas, A., Urrego, P., Ruiz-Verdú, A., Delegido, J., Tenjo, C., et al., 2019. Evaluation of atmospheric correction algorithms over Spanish inland waters for sentinel-2 multi spectral imagery data. Remote Sensing 11 (12), 1469.
Pendleton, L., Donato, D.C., Murray, B.C., Crooks, S., Jenkins, W.A., Sifleet, S., Craft, C., Fourqurean, J.W., Kauffman, J.B., Marbà, N., 2012. Estimating global "blue carbon" emissions from conversion and degradation of vegetated coastal ecosystems. PLoS ONE 7 (9), e43542.
Phinn, S., Roelfsema, C., Dekker, A., Brando, V., Anstee, J., 2008. Mapping seagrass species, cover and biomass in shallow waters: An assessment of satellite multi-spectral and airborne hyper-spectral imaging systems in Moreton Bay (Australia). Remote Sens. Environ. 112 (8), 3413–3425.
Phinn, S., Roelfsema, C., Kovacs, E., Canto, R., Lyons, M., Saunders, M., Maxwell, P., 2018. Mapping, Monitoring and Modelling Seagrass Using Remote Sensing Techniques. Seagrasses of Australia. https://doi.org/10.1007/978-3-319-71354-0_15.
Poursanidis, D., Topouzelis, K., Chrysoulakis, N., 2018. Mapping coastal marine habitats and delineating the deep limits of the Neptune's seagrass meadows using very high resolution Earth observation data. Int. J. Remote Sens. 39 (23), 8670–8687.
Poursanidis, D., Traganos, D., Reinartz, P., Chrysoulakis, N., 2019. On the use of Sentinel-2 for coastal habitat mapping and satellite-derived bathymetry estimation using downscaled coastal aerosol band. Int. J. Appl. Earth Obs. Geoinf. 80, 58–70.
Pu, R., Bell, S., 2017. Mapping seagrass coverage and spatial patterns with high spatial resolution IKONOS imagery. Int. J. Appl. Earth Obs. Geoinf. 54, 145–158.
R Core Team, 2019. R: A language and environment for statistical computing. R Foundation for Statistical Computing, Vienna, Austria https://www.R-project.org/.
Revillion, C., 2010. Spatialisation des activités et des prélèvements de la pêche artisanale sur le Parc National du Banc d'Arguin (Mauritanie). Thèse professionnelle SILAT, IRD - AgroParisTech - PNBA, Maison de la Télédétection, Montpellier, 33 p., annexes.
Revillion, C., Kide, A., Ould Yarba, L., 2011. Une base de données spatiales sur la pêche artisanale dans le Parc national du Banc d'Arguin (Mauritanie), outil au service d'une gestion durable de la ressource. Communication au Congrès international ICCAFFE, 19-21 mai 2011, Agadir, Maroc.
Rouse, J.W., Haas, R.H., Schell, J.A., Deering, D.W., 1974. In: Monitoring vegetation systems in the Great Plains with ERTS. NASA Special Publication, p. 309.
Romero, J., Lee, K.S., Pérez, M., Mateo, M.A., Alcoverro, T., 2006. Nutrient dynamics in seagrass ecosystems. *Seagrasses: Biol., Ecol. Conservat.* 227–254.
Schaffmeister, B.E., Hiddink, J.G., Wolff, W.J., 2006. Habitat use of shrimps in the intertidal and shallow subtidal seagrass beds of the tropical Banc d'Arguin, Mauritania. J. Sea Res. 55, 230–243.
Sevrin Reyssac, J., Richer de Forges, B., 1985. Particularités de la faune ichtyologique dans un milieu sursalé du parc national du banc d'Arguin (Mauritanie). Océanographie tropicale 20 (1), 85–90.
Short, F.T., Wyllie-Echeverria, S., 1996. Natural and human-induced disturbance of seagrasses. Environ. Conserv. 23 (1), 17–27.
Short, F. T., & Coles, R. G. (Eds.). (2001). Global seagrass research methods (Vol. 33). Elsevier.
Sòria-Perpinyà, X., Vicente, E., Urrego, P., Pereira-Sandoval, M., Tenjo, C., Ruíz-Verdú, A., et al., 2021. Validation of Water Quality Monitoring Algorithms for Sentinel-2 and Sentinel-3 in Mediterranean Inland Waters with In Situ Reflectance Data. Water 13 (5), 686.
Strydom, S., Murray, K., Wilson, S., Huntley, B., Rule, M., Heithaus, M., et al., 2020. Too hot to handle: Unprecedented seagrass death driven by marine heatwave in a World Heritage Area. Glob. Change Biol. 26 (6), 3525–3538.
Topouzelis, K., Makri, D., Stoupas, N., Papakonstantinou, A., Katsanevakis, S., 2018. Seagrass mapping in Greek territorial waters using Landsat-8 satellite images. Int. J. Appl. Earth Obs. Geoinf. 67, 98–113.
Traganos, D., Cerra, D., Reinartz, P., 2017. Cubesat-derived detection of seagrasses using planet imagery following unmixing-based denoising: Is small the next big? International Archives Photogrammetry, Remote Sensing Spatial Information Sciences-ISPRS Archives 42 (W1), 283–287.
Traganos, D., Reinartz, P., 2018. Mapping Mediterranean seagrasses with Sentinel-2 imagery. Mar. Pollut. Bull. 134, 197–209.
Traganos, D., Aggarwal, B., Poursanidis, D., Topouzelis, K., Chrysoulakis, N., Reinartz, P., 2018. Towards global-scale seagrass mapping and monitoring using Sentinel-2 on Google Earth Engine: The case study of the aegean and ionian seas. Remote Sensing 10 (8), 1227.
Trégarot, E., Failler, P., Maréchal, J.P., 2017. Evaluation of coastal and marine ecosystem services of Mayotte: Indirect use values of coral reefs and associated ecosystems. Int. J. Biodiversity Sci., Ecosyst. Services Manage. 13 (3), 19–34.
Trégarot, E., Catry, T., Pottier, A., Cornet, C., Maréchal, J.-P., Fayad, V., et al., 2018. Évaluation des services écosystémiques du Banc d'Arguin, Mauritanie. Report for the NationalPark of Banc d'Arguin.
Tucker, C.J., Elgin Jr, J.H., McMurtrey Iii, J.E., Fan, C.J., 1979. Monitoring corn and soybean crop development with hand-held radiometer spectral data. Remote Sens. Environ. 8 (3), 237–248.
Unsworth, R.F.K., Cullen-Unsworth, L.C., 2014. Biodiversity, ecosystem services, and the conservation of seagrass meadows. Coastal Conservat. 19, 95.
Vahtmäe, E., Kutser, T., Martin, G., Kotta, J., 2006. Feasibility of hyperspectral remote sensing for mapping benthic macroalgal cover in turbid coastal waters—a Baltic Sea case study. Remote Sens. Environ. 101 (3), 342–351.
Vahtmäe, E., Paavel, B., Kutser, T., 2020. How much benthic information can be retrieved with hyperspectral sensor from the optically complex coastal waters? J. Appl. Remote Sens. 14 (1), 016504.
Van Etten, J.P.C., 2003. Banc d'Arguin, a Nursery for fish species. Master thesis. University of Groningen.
Van der Laan, B., Wolff, W.J., 2006. Circular pools in the seagrass beds of the Banc d'Arguin, Mauritania, and their possible origin. Aquat Bot 84, 93–100.
Vanhellemont, Q., Ruddick, K., 2018. Atmospheric correction of metre-scale optical satellite data for inland and coastal water applications. Remote Sens. Environ. 216, 586–597.
Vanhellemont, Q., 2019. Adaptation of the dark spectrum fitting atmospheric correction for aquatic applications of the Landsat and Sentinel-2 archives. Remote Sens. Environ., 225, 175-192.
Vapnik, V. N., 1995. The nature of statistical learning theory. Springer-Verlag.
Ward, L.G., Kemp, W.M., Boynton, W.R., 1984. The influence of waves and seagrass communities on suspended particulates in an estuarine embayment. Marine Geol., 59, 85-103.
Waycott, M., Duarte, C.M., Carruthers, T.J., Orth, R.J., Dennison, W.C., Olyarnik, S., et al., 2009. Accelerating loss of seagrasses across the globe threatens coastal ecosystems. Proc. Natl. Acad. Sci. 106 (30), 12377–12381.
Williamson, D.F., Parker, R.A., Kendrick, J.S., 1989. The box plot: a simple visual method to interpret data. Ann. Intern. Med. 110 (11), 916–921.
Yang, D., Yin, X., Zhou, L., 2017. Seagrass distribution changes in Swan Lake of Shandong Peninsula from 1979 to 2009 inferred from satellite remote sensing data. Satellite Oceanogr. Meteorol. 2.
Zhang, C., 2015. Applying data fusion techniques for benthic habitat mapping and monitoring in a coral reef ecosystem. ISPRS J. Photogramm. Remote Sens. 104, 213–223.